CHALMERS
UNIVERSITY OF TECHNOLOGY

Curve squeal on the Stockholm metro

Statistical analysis based on data collected by an onboard monitoring system

Master's thesis in Sound and Vibration

ANNA ŚWIERKOSKA

Department of Civil and Environmental Engineering
CHALMERS UNIVERSITY OF TECHNOLOGY
Gothenburg, Sweden 2019

Master's thesis ACEX30-19-112

Curve squeal on the Stockholm metro

Statistical analysis based on data collected by an onboard monitoring system

ANNA ŚWIERKOSKA

Department of Civil and Environmental Engineering
Division of Applied Acoustics
Vibroacoustics Group
Chalmers University of Technology
Gothenburg, Sweden 2019

Curve squeal on the Stockholm metro
Statistical analysis based on data collected by an onboard monitoring system
ANNA ŚWIERKOSKA

Supervisor: Peter Torstersson, VTI
Examiner: Astrid Pieringer, Applied Acoustics

Master's Thesis ACEX30-19-112
Department of Civil and Environmental Engineering
Division of Applied Acoustics
Vibroacoustics group
Chalmers University of Technology
SE-412 96 Gothenburg
Telephone +46 31 772 1000

Cover: C20 2181 of SL (Storstockholms Lokaltrafik) at Stockholm, Sweden, photo by David Gubler, 2016

Typeset in LaTeX
Printed by Chalmers Reproservice
Gothenburg, Sweden 2019

Curve squeal on the Stockholm metro
Statistical analysis based on data collected by an onboard monitoring system
Master's Thesis in the Master's programme in Sound and Vibration
ANNA ŚWIERKOSKA
Department of Civil and Environmental Engineering
Division of Applied Acoustics
Vibroacoustics Group
Chalmers University of Technology

Abstract

Curve squeal is a high level tonal noise that is generated during curving of rail vehicles as a result of vibrations induced by the low rail (inner wheel) wheel–rail contact. Due to its large magnitude tonal components typically in the range up to 10 kHz, squeal is regarded to be the most annoying noise generated by the railway transport system. The mitigation of squeal noise is challenging and urgent as railway networks are often located in densely populated areas and rail-bound transportation is expected to become a backbone in the development of the future sustainable transportation system.

The current study is based on noise data recorded by an onboard monitoring system during one year of traffic on the green metro line of the Stockholm metro. The influence of selected variables on the generation of curve squeal are investigated by a statistical assessment performed in two steps; (1) a screening analysis accounting for the entire green metro line with focus on variables related to track alignment (e.g. curve radius and track constructed inside or outside of tunnels) and environmental conditions (e.g. time of year and precipitation) and (2) a detailed analysis of the conditions that promote squeal generation at two selected short radius curves exposed to severe curve squeal. For the later a third-order logistic regression model is developed with air temperature, humidity and vehicle speed as predictor variables. The results clearly show the generation of curve squeal to become more frequent with decreasing curve radius. For the two curves studied in the logistic regression analysis, vehicle speed is found to be unimportant with respect to squeal generation. In this part of the study only the coefficient related to humidity shows a significant influence on the origin of curve squeal. The importance of environmental conditions is further emphasised by the observation that the occurrence of curve squeal decreases during precipitation.

Keywords: Squeal noise, curve squeal, logistic regression

Acknowledgements

The project is performed in collaboration between Chalmers, Stockholm metro (SL) and the consultacy firm Tyréns. I would like to thank Astrid Pieringer of Chalmers University of Technology, who is my supervisor and also the examiner, Rickard Nilsson from SL, Martin Höjer from Tyréns and Olle Eriksson from VTI for all the documentation, data, help and advice when needed. Especially, I send sincerely thanks to my supervisor Peter Torstensson of the Swedish National Road and Transport Research Institute (VTI) for his great involvement not only in this work, but also in my professional growth.

Anna Świerkoska, Gothenburg, 2019

Contents

List of Figures

List of Tables

1 Introduction

Squeal is a high level tonal noise that may be generated while curving as a result of vibrations induced by the wheel–rail contact at the low rail (usually referred to as the "curve squeal") or high rail (usually referred to as the "flanging noise"). Due to its large magnitude tonal components (typically in the frequency range below 10 kHz), it is regarded as the most annoying noise generated by the railway system. The mitigation of squeal noise is challenging and urgent as railway networks often are located in densely populated areas and rail transport is expected to play a significant role in the development of the future sustainable transportation system. It is therefore of interest to deepen the knowledge about root causes of curve squeal generation and factors that influences its occurrence.

1.1 The structure of the study

The study consists of three parts, i.e. literature study, screening analysis and logistic regression analysis.

The necessary background to railway squeal noise is given in the literature study. It reviews literature on measurements performed in field and experimental test rigs and considers investigations on squeal noise mechanisms, its origin and features. In particular, variables that influence the occurrence of curve squeal but are not accounted for as part of the current work, e.g. friction coefficient, are discussed.

The method chapter describes how the data used in the current study have been collected and investigated by performing separate statistical screening and logistic regression analyses. The former considers the influence of operational (e.g. curve radius) and environmental (e.g. track constructed in or outside a tunnel, season of the year, temperature, precipitation) conditions on the generation of curve squeal. While in the later, a logistic regression model is developed for the prediction of curve squeal probability. The outcome of these studies is presented in the results chapter.

1.2 Limitations

No measurements were performed as a part of the current project. Therefore, the content of the work is based on the data collected by the on-board noise monitoring system used on the Stockholm metro. These data were provided to the project by Stockholm metro and the consultancy firm Tyréns solutions. The current work is focused on generation of curve squeal along the Green line at Stockholm metro. Other types of squeal noise such as flanging noise or brake squeal are not considered.

2

Literature study

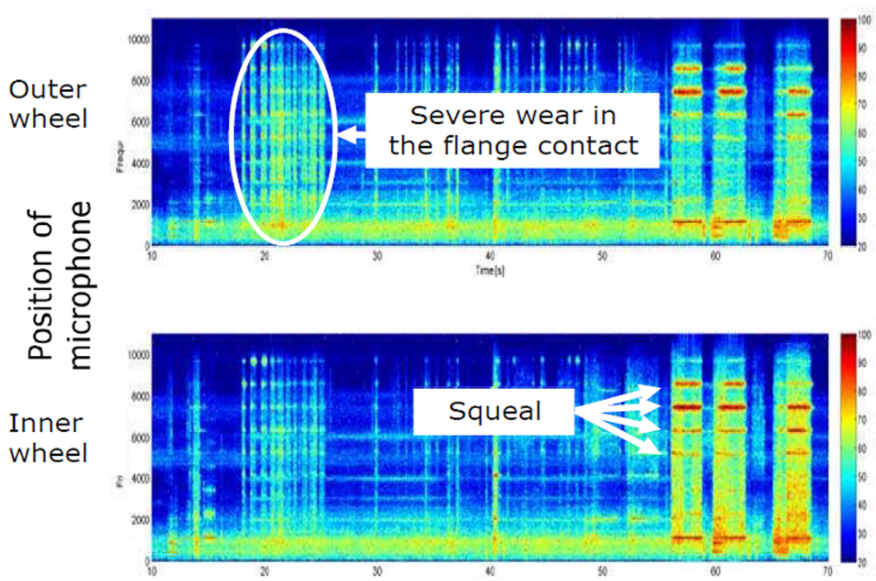

Figure 2.1: Spectrogram containing squeal and flanging noise [2]

Squeal is a tonal noise dominated by a single frequency at a sound pressure level typically more than 20 dB above the rolling noise level, [1], see Figure 2.1. The dominant squealing frequencies vary between different experiments [3]. As illustrated in Figure 2.2, squeal is usually dominated by a peak sound pressure level at one or two frequencies, that do not necessarily correspond to the lowest modes [4]. According to Thompson [5], tonal components of squeal are generally in the range between 250 Hz and 5 kHz. Thus, it can be stated, that they are always in a range, at which human hearing is the most sensitive, see Figure 2.3. This, together with its strong tonality and high sound pressure levels makes squeal the most annoying noise emitted during railway traffic.

Another event revealed in the spectrogram in Figure 2.1 is flanging noise, which usually has a more broadband frequency characteristics and is less intense than squeal. In [6], flanging noise is identified to cover the frequency range above 5 kHz.

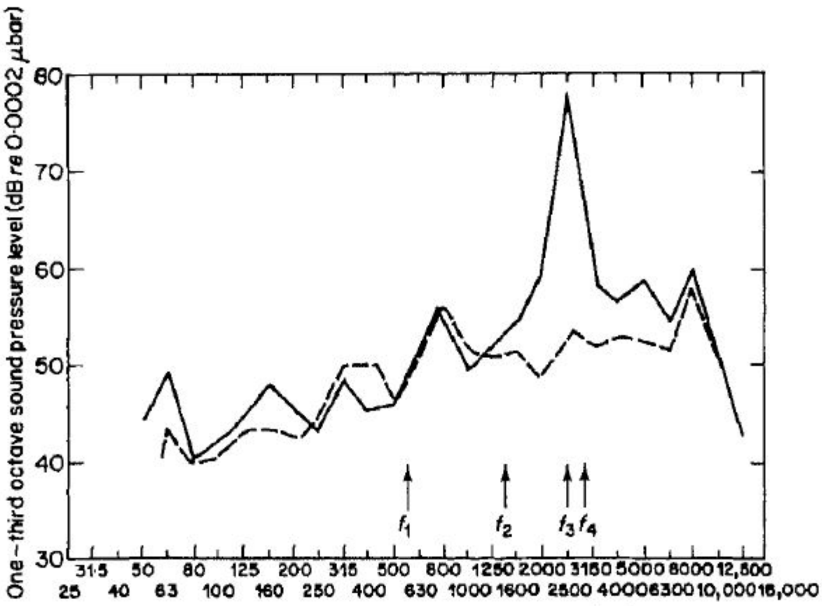

Figure 2.2: Frequency characteristics of squeal measured at the Transportation Test Center, Colorado with the SOAC car. Solid line - squeal, dashed line - no squeal. Indicated natural frequencies of the wheel, f1 - f4 [4]

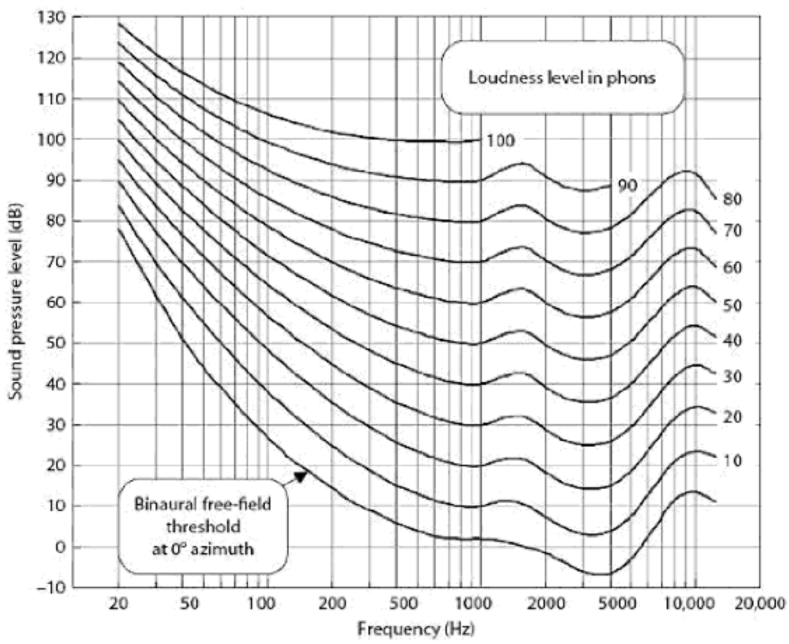

Figure 2.3: Equal-loudness level contours from ISO 226:2003 [7]

The variability and non-repeatability of squeal makes it difficult to examine. The occurrence of squeal is dependent on many factors and measured sound pressure levels may vary from one event to another even though the conditions are nominally identical. Additionally, squeal is often intermittent [4, 8], meaning that during one event it alternately ceases and starts again. Figure 2.4 illustrates this by showing the difference between measured maximum and energy-averaged sound levels of squeal. In order to express the squeal noise reduction, the rate of occurrence and duration should be considered in addition to noise reduction expressed in dB that is a standard for other noise types [9]. Several methods to identify curve squeal and flanging noise have been developed. Most of the algorithms are spectrally-based and assume that the sound pressure level during squealing exceeds that for rolling noise with around 10 - 20 dB and that the most of the energy is contained in tonal components usually between 1 - 10 kHz. More complex pattern-recognition-based algorithms are also developed. Although, curve squeal is often successfully detected, there is still a need to establish an effective algorithm for flanging noise recognition [10].

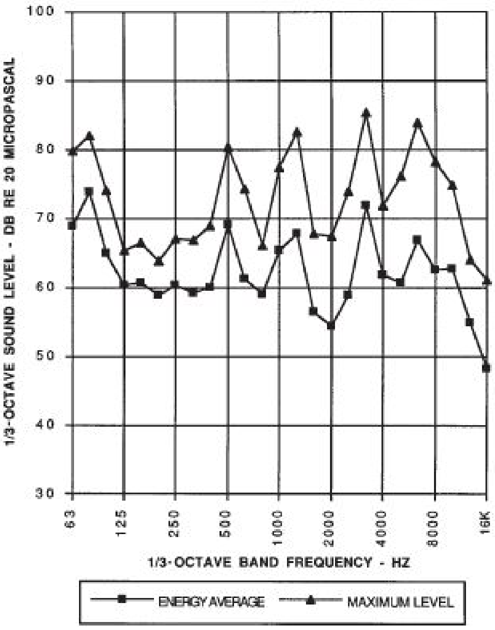

Figure 2.4: Results of wheel squeal at Portland TriMet on a 26.5 m radius curve [8]

2.1 Squealing conditions

Curve squeal might be seen as a result of a “flawed” behaviour during curve negotiation of rail vehicles. A negative friction slope with respect to the lateral creepage under full sliding is widely recognised as the main principle leading to squeal and has been used in many studies in literature [12, 5]. However, mode coupling, also known as flutter, is considered to be another convincing explanation that has earned a more recent recognition.

2.1.1 Curving behaviour

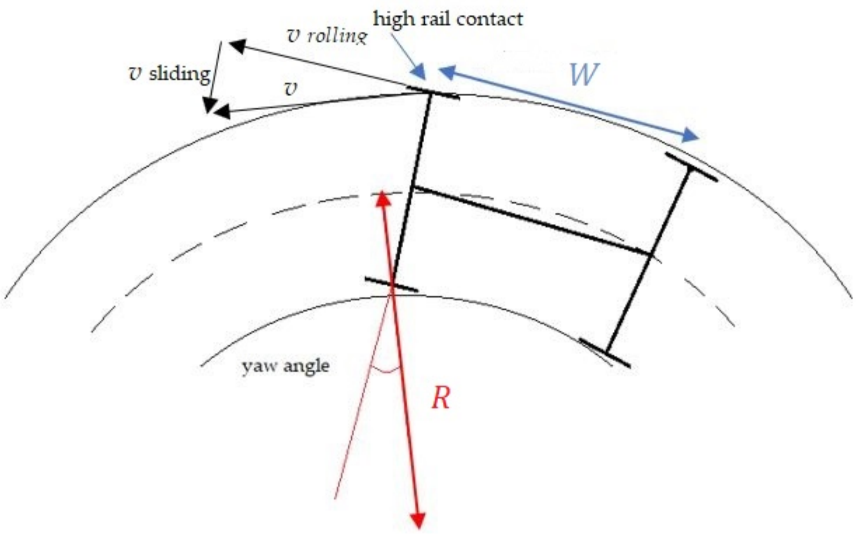

Figure 2.5: Illustration of a train bogie negotiating a small radius curve. The yaw angle of the under-radially steering leading wheelset and the associated sliding velocities developed in the high-rail contact are outlined. Similar figure as in e.g. [3, 4]. R is the curve radius and W is the wheelbase.

When two wheels of the same axle steer around a curve, the outer wheel needs to travel a longer distance than the inner wheel. This is compensated by the rolling radius difference between the wheels, which is due to its conical geometry. An unsuspended wheelset can align itself radially when negotiating a curve, this is referred to as an ability to radially steer. However, for a rail vehicle to have a stable running behaviour at high speeds, wheelsets need to be resiliently attached to a bogie frame. Except for large radius curves, this design has the unwanted consequence to prevent wheelsets to align radially in curves [11]. The definition of large or small curve radius depends on a specific vehicle’s curving ability, e.g. in [12], radius above 600 m is considered large. In result, wheelsets develop a non-zero yaw angle (also called angle-of-attack). This corresponds to the angle between the wheel axle and the radial direction of the circular curve as shown in Figure 2.5. A relative lateral sliding velocity between the wheel and the rail is generated as indicated in the same figure, see $v_{sliding}$. The relative velocity normalised by the rolling velocity is called creepage. As a reaction, creep forces are created with a direction opposite to the creepage [5]. For a leading wheelset in a curve, the angle of attack may be large and creep forces act mainly in the lateral direction as presented in Figure 2.6. At the trailing wheelset the situation is different with a small angle of attack that make forces more aligned with the longitudinal direction.

In [12] Rudd shows that although the rail is excited and vibrates at the squealing frequency, it is the wheel that is the most efficient radiator due to its lower impedance. Moreover, it is efficiently excited by the lateral creep forces acting in the axial direction with respect to the wheel (normal-to-wheel plane).

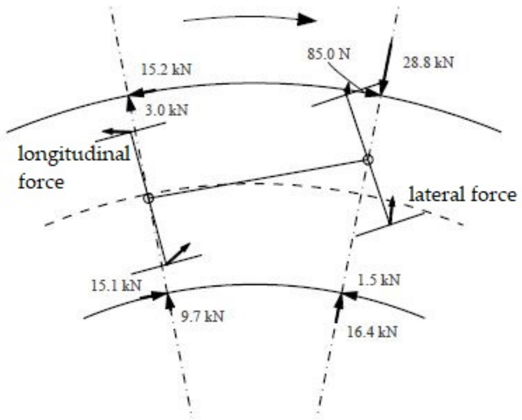

Figure 2.6: Example of creep forces developed during curve negotiation of a rail vehicle in a small radius curve. Forces outlined on the wheels and rails are in the wheel—rail contact plane and track plane, respectively [13]. Outlined forces act on the vehicle.

In the following, a few terms used to describe the track geometry (alignment) that are relevant for the current study are introduced. In order to reduce the effect of centrifugal acceleration while a vehicle is negotiating a curve, the outer rail is typically superelevated. This is also called cant. For canted curves, the inner and outer rails are also called low and high, respectively. For a given superelevation and curve radius, an equilibrium speed can be defined, which is the speed for which the lateral acceleration in the track plane is zero. Curve radius is related to the centre of the track and on circular curves, the radius is constant, while in case of transition curves, the radius as well as the cant are changed continuously [14].

2.1.2 Falling friction

The mechanism of curve squeal that has attracted the largest attention by the research community was introduced by Rudd as crabbing and is commonly referred to as "velocity-dependent friction" or "falling friction" [12].

In tight curves, the lateral creepage may reach large magnitudes and sliding of the entire wheel – rail contact can occur. This is referred to as saturated creep conditions. In the saturated region, unstable dynamic behaviour can be caused by the falling friction [5]. Vibrations corresponding to a stick-slip motion are then induced with a positive loss factor corresponding to an energy input per vibration cycle as described in [12]. As a result, vibrations become amplified leading to squeal [8]. The friction coefficient as a function of creepage is presented in Figure 2.7. At creepages that exceed that associated with the peak in friction magnitude (saturation), the friction coefficient starts to decrease and unstable vibrations might be generated. Their occurrence depends on the negative gradient of the friction-creepage slope [8]. At creepages below saturation, this gradient is positive and the mechanical system is stable. In [8] a simplified criterion for conditions that promote squeal is presented. This uses a simplistic equation to calculate the creepage as $\delta = 0.7\frac{W}{R}$ and in combination with Figure 2.7 it suggests that squeal does not occur when the ratio between the wheelbase W and curve radius R is less than approximately 0.01.

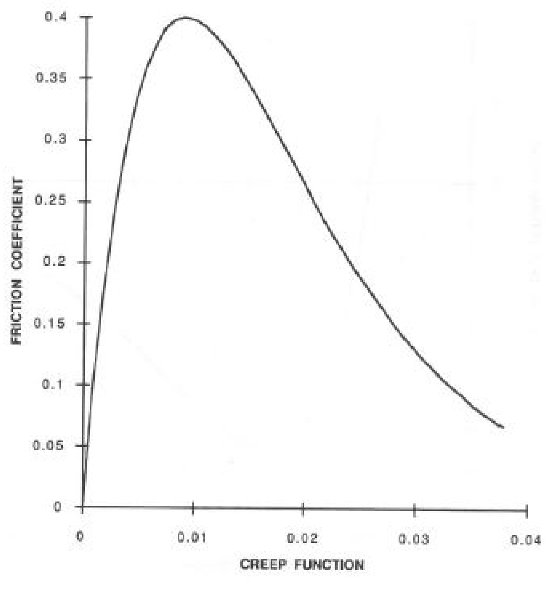

Figure 2.7: Illustration of friction-creepage curve [8], given from Rudd's expression in [12]

2.1.3 Mode coupling

It has been discovered that even for cases with a constant wheel–rail friction after saturation, the wheel–rail system might still be unstable and produce squeal. To this end, another possible squeal mechanism called "mode coupling" has been demonstrated. The instability arises at a frequency determined by two coupled eigenmodes of the vehicle–track system. In the case of large radius curves, the dominant mechanism responsible for the generation of curve squeal was found to be longitudinal creep and modal coupling [15]. In [16] an investigation on curve squeal, that includes both measurements and simulations accounting for both the falling friction and mode coupling excitation mechanism is presented. For the case of constant wheel–rail friction, two typical features of mode coupling are observed: a difference between natural frequencies of the wheel and the squealing frequency, and a phase shift between vertical and lateral vibrations. This phase lag becomes smaller when introducing a negative friction slope in the model and is not observed when the negative friction slope becomes the dominant excitation mechanism.

2.2 Measurements

According to the measurement proposal in [17], following variables influence the generation of curve squeal: the ratio between the wheelbase and the curve radius, magnitude of wheel–rail creep forces, wheel and rail transverse profiles, cant, track gauge, flange distance, temperature and humidity of the railhead, and parameters coupled to the structural flexibility of wheel and rail (e.g. modal stiffness and damping). In the above, the ratio between the wheelbase and the curve radius is interpreted as the angle of attack, which is directly related to the wheel–rail creep force [17]. According to [4], the lateral creepage developed during curving is mainly determined by the geometry of the curve and the bogie, and can be approximated to lie between the ratio $\frac{W}{R}$ and $\frac{W}{2R}$, where W is the wheelbase and R is the curve radius.

In the following, studies that contain measurements of railway squeal noise performed in experimental test-rigs or in-field are reviewed. The results for the identified main significant parameters are presented in separate subsections. Additionally, a few interesting observations found in the literature are listed below:

- Due to the change in friction characteristics, wheel squeal may be reduced significantly during wet weather conditions [8]

- In [18], curve squeal generated from freight trains is investigated. The results indicated that the axle load does not influence the occurrence of squeal. Moreover it was found that wagons permanently coupled were more prone to squeal compared to wagons with an automatic coupling. Only a few wagons of a complete train set squeal, however these were located in the front, middle and rear of trains [18]

- In [19], curve squeal was not generated when the wheel was in flange contact with rail.

2.2.1 Which wheel is squealing?

Although most researchers agree that squeal originates from the inner wheel, results from field measurements also provide diverging observations. In [20], field measurements on the Paris metro and on the tramway in Grenoble are reported. For a metro bogie negotiating a 75 m radius curve, the maximum sound pressure levels were measured for the leading inner wheel. At lower speeds (10 km/h and 20 km/h) also the inner wheel of the trailing wheelset squealed but at a lower sound pressure level. For the tramway passing a curve of radius 60 m at low speed, the inner wheel of the leading wheelsets of both leading and trailing bogie squealed. At higher vehicle speed squeal was generated from the high rail contact of the rear wheelset in the trailing bogie.
During 9 days of noise monitoring on a 284 m radius curve on the Sydney metro, squeal was found to originate mostly from the high rail [21]. Another example is based on data captured during over 2.5 years with a permanent noise detector located at Heathfield, UK. It consisted of an array of microphones placed 6 m from the low rail. A detailed analysis of the large data-set revealed both curve squeal and flanging noise events generated from the leading wheelset of leading bogies [22].

2.2.2 Wheel–rail friction

In the in-situ conditions, it is hardly possible to measure lateral forces and consequently, friction. Therefore, most of the conclusions are based on the results from experimental measurements. In [3], several experiments on a reduced scale rig considering lateral creep and curve squeal while measuring friction are summarised. Most of them reported squeal in presence of falling friction. In two cases, squeal was found in the absence of falling friction.

In the experiment described in [23], a 1/3 scale model of an undamped wheel running on a second damped wheel representing the rail was used. Figure 2.8 shows friction coefficient with respect to the angle of attack, considering the occurrence of squeal. Squeal was generated for angles above 0.4^o corresponding to a creepage of 0.7 %. In this region, friction coefficient decreases with respect to creepage.

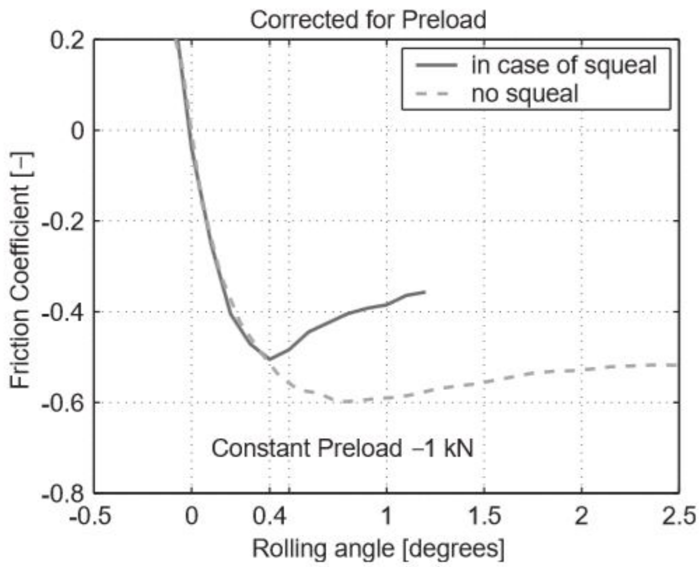

Figure 2.8: Occurrence of squeal for two different friction conditions. Results obtained in a 1/3 scale experimental twin disc rig [23]

An experimental test rig with a 1/4 scale reproduction of a MF77 rolling-stock wheelset and two rails with profile and gauge equivalent to a 1/4 scale track with UIC60 rails mounted on the circumference was used in a French research project concerning curve squeal reduction on urban railways [19], see Figure 2.9. Mean lateral forces applied to the axle together with the angle of attack and the average wheel–rail lateral friction coefficient in dry and wet conditions (water sprayed on the rail) were measured.

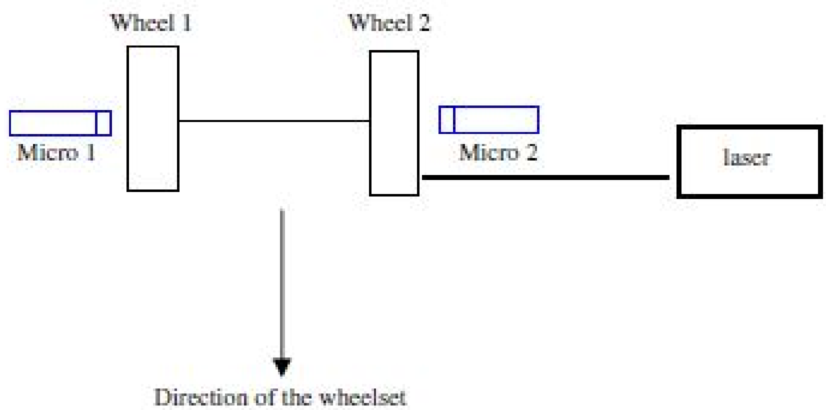

Figure 2.9: Illustration of the 1/4 scale wheelset used in the experiment presented in [19]

An example result from [19] showing the measured friction versus angle of attack is presented in Figure 2.10. Both for wet and dry conditions, three separate regions were identified in these functions; (1) for small angles of attack (referred to by the authors as the "creep area"), friction is found to be proportional to the angle of attack, (2) at intermediate angles of attack in the transitional part (referred to by the authors as the "saturated area") full sliding occurs, for dry and wet conditions this regions starts at 8 mrad and 4 mrad, respectively, (3) the friction coefficient was constant for increasing creep values. Although, in this area no negative slope was observed, squeal was consistently generated under dry conditions. It should be highlighted that in contrast to the instantaneous friction law that is applied in theoretical models, here the quasi-static friction averaged over several wheel vibrating cycles was measured [19]. A similar example is reported in [24], where different friction modifiers were applied to a rolling contact twin-disc experimental rig. Squeal was present despite the experimentally observed quasi-static positive slope of friction with respect to creepage. This is proposed to be due to an increase in temperature for large magnitude lateral velocity, which causes an increase in friction coefficient and a shift of the instantaneous friction curve, which still may have a negative slope [24].

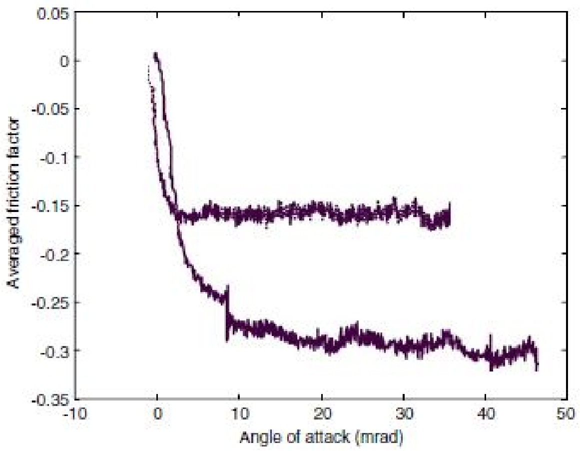

Figure 2.10: Average friction coefficient with respect to the angle of attack. Solid line (bottom) - dry, dashed line (top) – wet conditions [19]

Many field measurements of wheel–rail friction are focused on the effectiveness of lubrication and friction modifiers as a mitigation action. The latter is a material that added to the wheel–rail contact surface changes the friction condition relative to dry steel–steel contact in a way that prevents a negative slope between friction and creepage. They are also referred to as High Positive Friction (HPF) and are applied on the wheel tread. There are also products referred to as Low Coefficient of Friction (LCF) that are applied on the flange of the wheel in order to control flange and gauge face wear [8]. Friction modifiers are distinct from lubrication products, that may be any substance intended to reduce the friction coefficient [9]. Squeal noise generated from a 17.5 m radius curve on the tram in Milan was measured in 2013 [25]. The traffic consisted of modern articulated vehicles with resilient wheels. The influence of the friction coefficient on the generation of squeal was investigated by comparison of sound pressure levels measured for dry and wet track, see Figure 2.11. For wet contact conditions, a decrease in the global sound pressure level as well as in the frequency band 1.4 - 1.8 kHz, compared to dry conditions was observed. This means that squeal was eliminated [25].

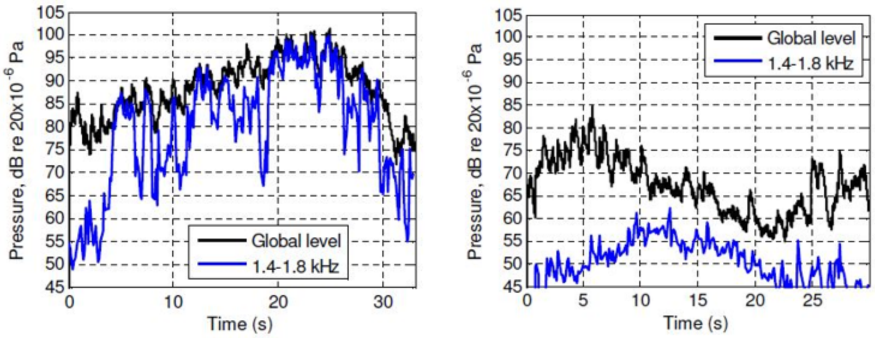

Figure 2.11: Sound pressure level measured during curve negotiation of a tram vehicle through a 17.5 m radius curve on Milan tramways. Vehicle speed 10 km/h. Left - dry track, right – wet track [25]

The relative humidity influences creepage. In [26] it was reported that the critical creepage (creepage point at which friction coefficient starts to fall) decreases with increasing relative humidity. In [27], in-field measurements performed on a 300 m radius curve of a suburban railway site in Australia revealed that the probability of squeal increases with increasing relative humidity. The measurement data as well as the meteorological data was collected for a period of one year. The results are presented in Figure 2.12.

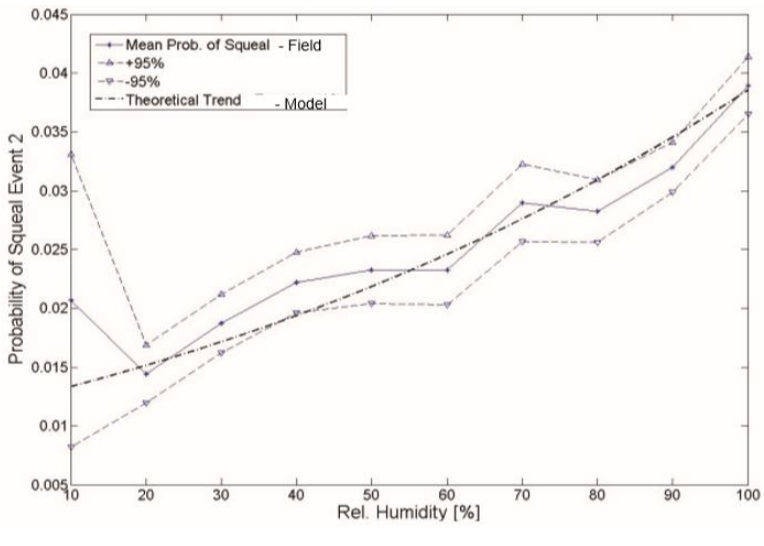

Figure 2.12: Predicted and measured effect of relative humidity on the probability for squeal. Confidence intervals are outlined [27]

An interesting observation was made at Barnt Green, where the lubrication system was recognized as an effective squeal mitigation measure only during short periods and not during rainfall according to complaints by residents [28].

The performance of a water–based friction modifier on two underground metro systems is evaluated in [6]. Friction coefficient after the application of the substance is controlled in a range between 0.35 and 0.4. The results are presented in Figures 2.13 and 2.14. Although the spectra are rather flat, which may indicate a significant broad band contribution due to the rolling noise, curve squeal is also present [6]. The reviewed campaign considered also tests on tram and freight systems. The results in Figure 2.15 reveal a similar performance of the tested friction modifier for all different railway systems. Although the equivalent weighted sound pressure level is reduced, the results do not specify if the occurrence of squeal was also reduced after the application of friction modifier.

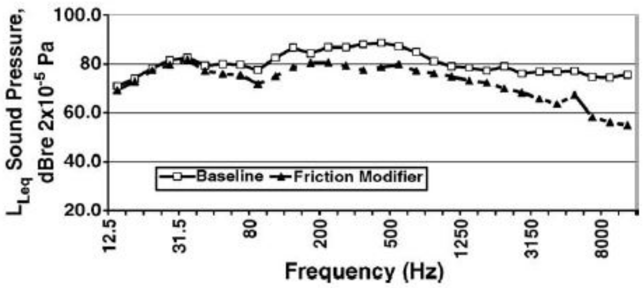

Figure 2.13: Sound pressure levels measured in-field for the case with and without low rail friction modification. Curve radius 97 m and vehicle speed of 8 km/h [6]

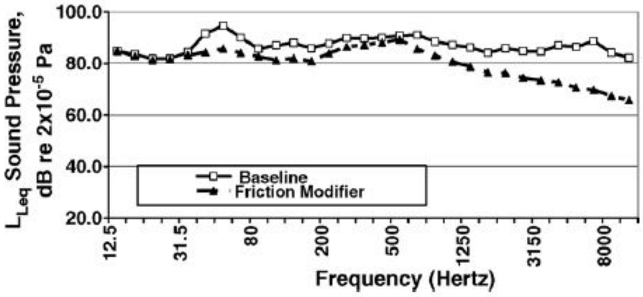

Figure 2.14: Sound pressure levels measured in-field for the case with and without low rail friction modification. Curve radius 90 m and vehicle speed of 32 km/h [6]

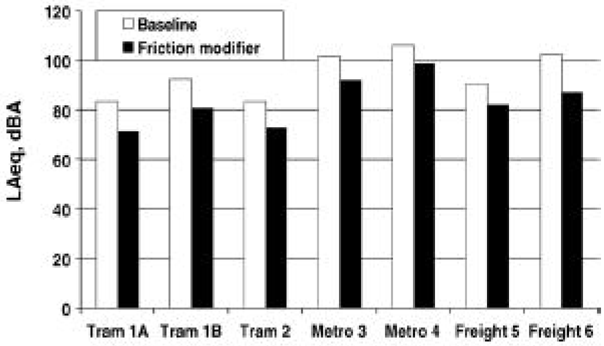

Figure 2.15: Equivalent continuous A-weighted sound levels measured in curves located on 6 different railway systems before and after the application of low rail friction modifier [6]

The influence of top-of-rail friction modification applied on the low rail of a 315 m radius curve in Teralba, Australia, was measured during 3 months [18]. The traffic consisted of both freight and passenger vehicles with speed limit 75 km/h. The results show that only freight trains squeal and that the performance of the friction modifier depends on the operator and type of train (e.g. steel product trains, coal, container trains). The summary of the results covering four descriptive categories of squeal ("no squeal", "mild", "moderate", "high") is presented in Figure 2.16. The proportion of severe squeals was reduced to around 35 % when the friction modifier was applied. Despite the measured improvement, friction modification was not found to be an effective solution to the squeal noise issue at the current site [18].

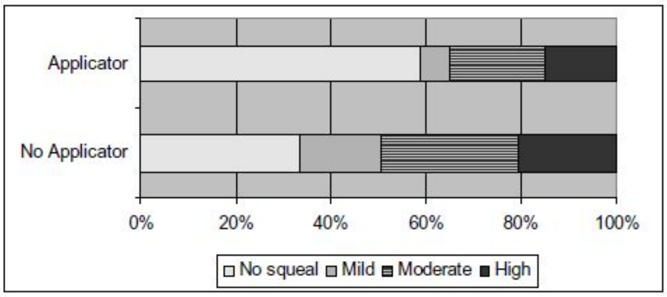

Figure 2.16: Squeal noise measured on a 315 m radius curve with mixed freight and passenger traffic. Comparison between results obtained with and without application of top-of-rail friction modification. Vehicle speed 75 km/h [18]

2.2.3 Wheel damping

Squeal noise reduction can be achieved with an appropriate wheel structural damping loss factor that guarantees the stability of the system also in conditions with a falling friction coefficient [3]. In [19] a minimal damping loss factor between 1.3 - 3 % was measured to avoid squeal at the specific wheel eigenmode. However, if mode coupling is present, the increase in damping does not necessarily provide stability. This is illustrated in Figure 2.17 with the stability map introduced by Thompson et al. in [3].

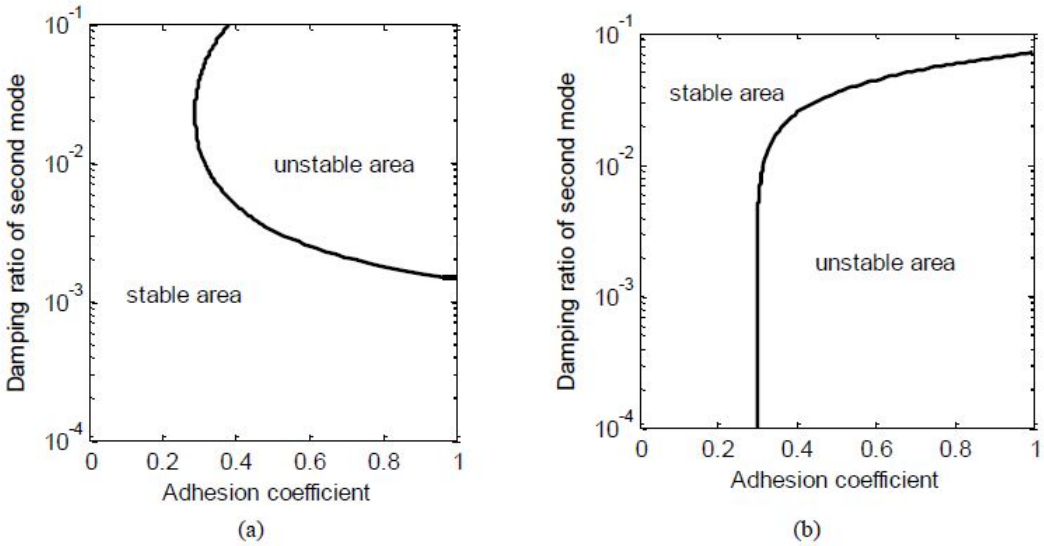

Figure 2.17: Effect of the damping ratio shown on stability maps for varying friction coefficient. A system considers two modes: a) damping ratio of the 2nd eigenmode is changed, stable region at low ratios of damping, b) damping ratio of both eigenmodes change (keeping their ratio fixed), stable region at damping ratios larger than 10^{-2} [3]

2.2.4 Bogie and track geometry. Angle of attack.

For a large enough radius, curve squeal is not likely to occur. However, it is not only the curve radius that should be considered but also the curving ability of the vehicle. As described in Section 2.2.2., the ratio between the wheelbase and the curve radius was approximated as the lateral creepage. However, by the definition, creepage is the ratio between the sliding and rolling velocity. Based on the measurements in [4] and calculations in [12], the rule of thumb was developed that squeal should not occur if the curve radius exceeds a factor 100 of the bogie wheelbase [4]. Experiments performed on the 1/4 scale test rig illustrated in Figure 2.9, showed squeal noise to stop for large magnitudes of lateral creepage (angle of attack larger than 20 mrad) due to flange contact [19]. An increase in sound pressure level of squeal with increasing angle of attack was observed. Additionally, squeal noise sound pressure levels were lower for positive compared to negative angles of attack due to flange contact for angles 20 - 25 mrad on this side [19], see Figure 2.18.

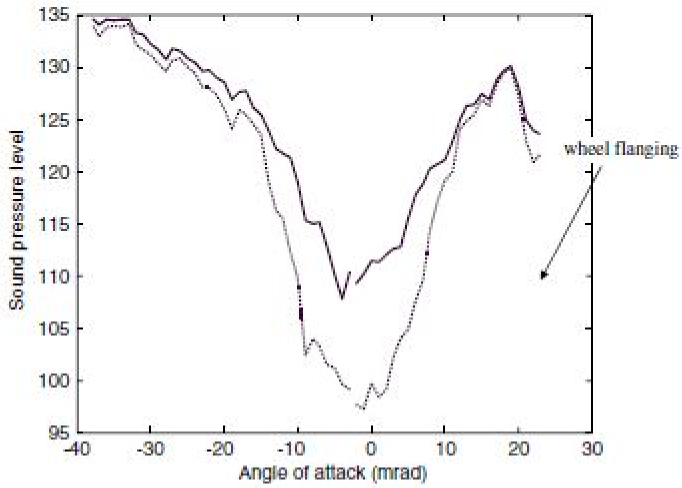

Figure 2.18: Sound pressure level measured with microphone 1 in the experimental setup illustrated in Figure 2.9 as a function of angle of attack. Rolling speed corresponding to 20 km/h. Sound pressure level in the frequency range 1 - 10 kHz (solid line) and 1.6 - 1.8 kHz (dashed line) [19]

In-field measurements of squeal noise performed predominantly on freight trains trafficking on the main north rail line in Sydney are presented in [22]. Results indicate that high squeal noise levels are generated at large angles of attack, see Figure 2.19.

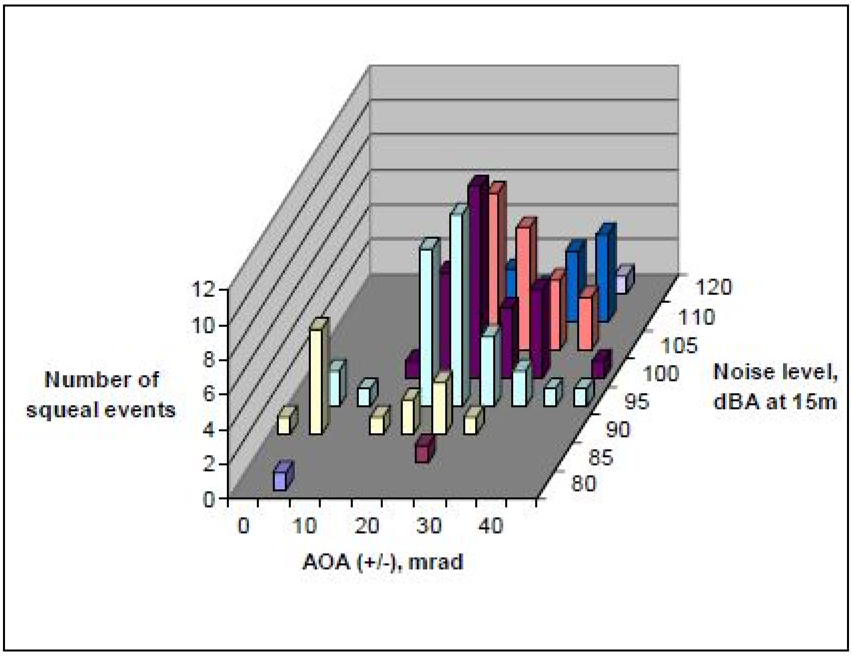

Figure 2.19: Summary of squeal noise measurements performed on the main north line in Sydney. Predominantly freight traffic [22]

The wheel and rail transverse surface geometry, i.e. the profiles, are essential for the generation of damage in the wheel–rail contact [29]. Desired wheel–rail contact conditions typically requires regular rail grinding. Potentially, a rail gauge corner geometry adopted for the application of lubrication can be implemented [1]. The effect of this on generation of curve squeal is illustrated in Figure 2.20.

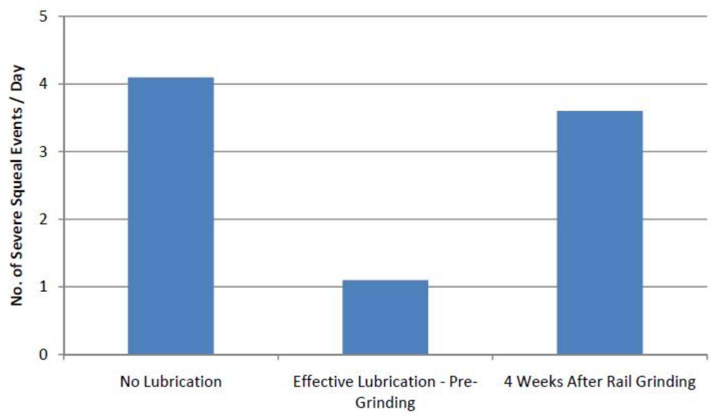

Figure 2.20: The effect of lubrication and rail grinding on curve squeal generation on a 300 m radius curve [1]

2.2.5 Sleepers

Upgrading sleepers from timber to concrete appears to be a factor responsible for the squeal noise issue expansion reported in [1]. The results of measurements conducted before and after retrofitting wooden with concrete sleepers on a 320 m radius curve located 125 km north of Sydney that carries both freight and passenger traffic show a considerable increase in squeal noise levels and occurrence rate [18]. The summary of the results covering four descriptive categories of squeal ("no squeal", "mild", "moderate", "high") is presented in Figure 2.21. No information considering a possible change in track gauge or fastening system was reported in the article.

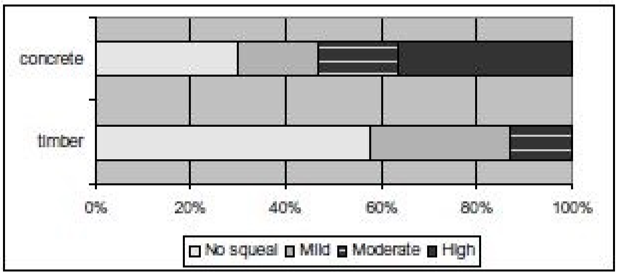

Figure 2.21: Summary of the measurement results from before and after retrofitting timber sleepers 54 kg/m with concrete sleepers 60 kg/m [18]

2.2.6 Vehicle speed

In-field measurements on a 75 m radius curve at the Paris metro are reported in [20]. Noise measured at four different vehicle speeds (10, 20, 30 and 40 km/h) as well as in the experimental test rig presented in Figure 2.9, showed that the sound pressure level of squeal increased with higher rolling velocity.

Measurements carried out on the 315 m radius curve in Teralba, Australia, do not show any beneficial effect with respect to the generated squeal noise from a reduction in vehicle speed from 75 km/h to 40 km/h. Moreover, the duration of squeal was longer in case of the lower vehicle speed which might increase the annoyance of residents living close to the track. The summary of results covering four descriptive categories of squeal ("no squeal", "mild", "moderate", "high") is presented in Figure 2.22. An interesting observation is that superelevation seemed to influence the occurrence of curve squeal, as there were differences between results obtained for tracks in opposite directions [18]. The squeal noise monitoring in Heathfield [7] has also shown a moderate correlation between vehicle speed and curve squeal and flanging noise levels, see Section 2.2.1.

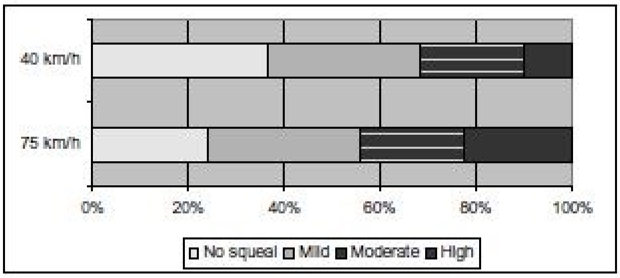

Figure 2.22: Summary of squeal noise measured for two different vehicle speeds on a 315 m radius curve located in Teralba, Australia [18]

2.3 Mitigation measures

Mitigation strategies against squeal noise should focus on reducing its occurrence rather than its radiated sound pressure level with means such as e.g. barriers [5]. Numerous experiments have been performed in order to test the effectiveness of different mitigation measures. Some of them have already been presented in the previous section. No measurement standard has been defined which means that different evaluation methods are used for different tests. An example representation of results is shown in Figure 2.23. The histogram presents the distribution of squeal events versus the maximum sound pressure levels [28].

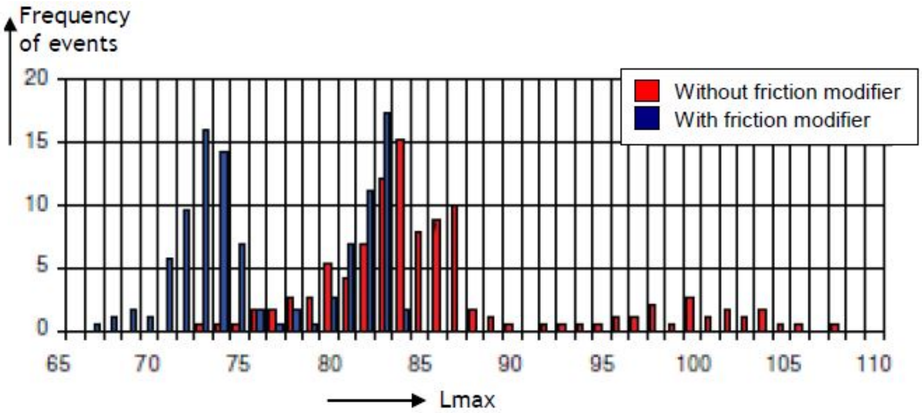

Figure 2.23: Distribution of squeal events verses maximum sound pressure levels. Test performed on the Berlin Ringbahn [28]

Some potential mitigation actions are only assessed at a specific situation. The lack of long-term monitoring in various locations makes their performance difficult to evaluate [9]. In [22], curve squeal is subdivided into three types: friction controlled, steering controlled and systemic which is featured by relatively high proportion of axles that squeal. It is noted that the success of the applied mitigation measure depends on features that are exhibited by a specific squeal type, i.e. friction controlled curve squeal is usually moderate and this noise can be effectively reduced or eliminated by applying top of rail friction modification, while in case of the steering controlled severe squeal, this solution hardly provides an improvement. For systemic squeal, lubrication may be the most appropriate mitigation action.

3

Method

The project is conceptually divided into two parts. The first part is a screening assessment. Its purpose is to analyse data concerning squeal events, detected by the track condition monitoring system used at the Stockholm metro (SL) and reported in the associated cloud service provided by Tyréns. In the second part, a logistic regression model is developed based on the raw measurement data. In this chapter, the condition monitoring system at SL, procedures used to perform the statistical screening analysis and the logistic regression are described.

3.1 Track condition monitoring system at Stockholm metro

The condition monitoring system used at SL is provided by the consultancy firm Tyréns under the product name “Quiet Track Monitoring System (QTMS)”. It has its origin in the European financed project "Quiet track" [30]. The objective of this project was to develop an efficient and optimised track maintenance by continuous monitoring of sound pressure level and acceleration [31]. Currently at SL, the condition of three metro lines is monitored by on-board systems mounted on seven trains of type C20 manufactured by Bombardier Transportation [32] (three vehicles on the green line and two on the blue and red line, respectively). The three metro lines are presented in Figure 3.1.

Figure 3.1: A schematic map of the metro system at Stockholm

The following information is provided by the condition health monitoring system:

- Track roughness
- Sound pressure
- Track decay rate
- Pad stiffness
- Severe wear
- Wheel slip
- Curve squeal

Quantities that are of particular interest in the current project are sound pressure and curve squeal. Hence, procedures and measurements used by the monitoring system to obtain all other results are not described as a part of the current work. The setup for on-board noise measurements is described in more detail in the following section.

3.1.1 Measurement setup

Microphones are mounted behind the leading bogie of the leading car or in front of the trailing bogie of the trailing car for a C20 trainset travelling in north- or southbound direction. The instrumented car may be turned at a train terminal, therefore, the location of microphones with respect to low and high–rail is not known from the provided data. The microphone setup is presented in Figure 3.2. In case the instrumented bogie is leading, two microphones are located close to the trailing axle (Mic 1 and Mic 2) and two microphones are mounted at a distance from this wheelset, in the middle of the car between two bogies (Mic 3 and Mic 4), see Figure 3.2. Noise recorded with microphones 1 and 2 is of particular interest in the current project, as it corresponds to the wheel/rail contact. The microphone sensitivity is 50 mV/Pa.

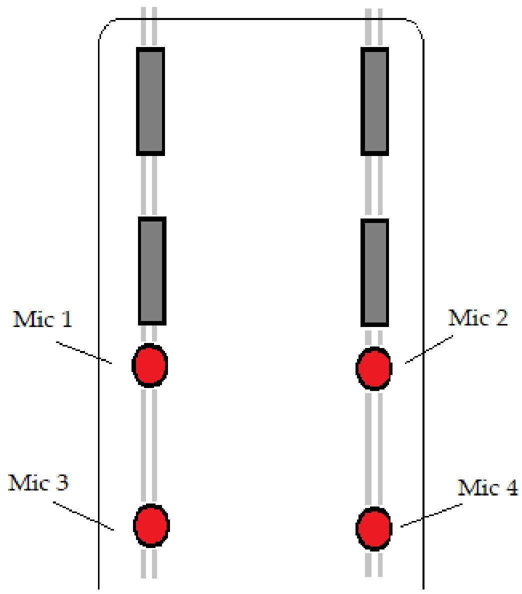

Figure 3.2: Microphone setup on a car

3.1.2 Squeal detection criterion

The algorithm used by the track condition monitoring system detects squeal when the following conditions are fulfilled:

- A vehicle is negotiating a curve
- Sound pressure level exceeds 95 dB (a vehicle is running)

- The noise radiation is dominated by the inner wheel–rail contact: sound pressure level at the inner wheel exceeds that at the outer wheel by at least 3 dBA

Curve squeal is assumed to be generated only by the inner wheel–rail contact. Hence, the final condition implies that squeal radiated from the outer wheel (flange squeal) is not counted as an "squeal event" by the system.

3.1.3 Raw measurement data

The raw data provided by the QTMS consists of five-minutes recordings in the compressed audio format FLAC (Free Lossless Audio Codec). Linked to each such audio recording a Matlab file is created including time, vehicle speed, curve squeal classification and location given as the distance from the reference station (Slussen) in meters and GPS coordinates. In the current work, data collected on selected curves of the green line during the period from August 25, 2017, to November 30, 2018 was included. In addition, documentation about track alignment, location inside or outside the tunnels and potential application of lubrication was provided by SL. Meteorological data includes temperature and humidity measured every hour at the station Stockholm - Bromma Airport. Missing temperature and humidity data samples, were replaced by interpolation between the closest data points and with data available from the website of the Swedish Meteorological and Hydrological Institute (SMHI) [36], respectively.

3.1.4 Curve selected for detailed analysis

Data recorded on the northbound track of a curve between stations Alvik and Stora mossen on the green line of SL was used for a detailed statistical analysis. The radius and length of the curve is 122.6 m and 120.550 m, respectively. It is located at the track following coordinates between 8475-8650 m from the reference at Slussen station, see Figure 3.5. The speed limit in the curve is 40 km/h. There is no high-rail lubrication applied. Additionally, a neighbouring curve with a radius of 318 m and the length of 175 m was analysed. It is located at the track following coordinates between 8700-8875 m from the reference at Slussen station, see Figure 3.6. The speed limit in the curve is 45 km/h. High-rail lubrication is applied at 7738 m from reference at Slussen station. Both curves are located outside the tunnels, see Figure 3.3 - 3.4. The traffic consists exclusively of C20 trains manufactured of Bombardier transportation [32].

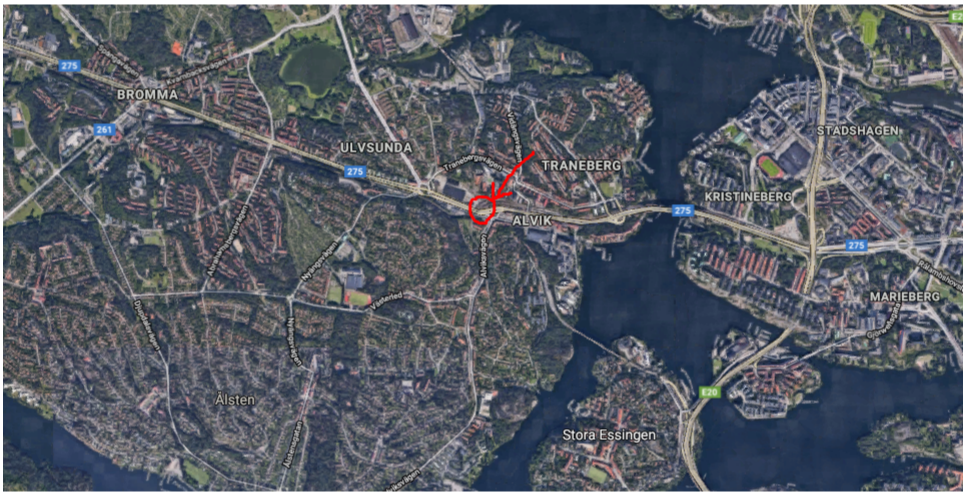

Figure 3.3: Location of chosen curves on the map

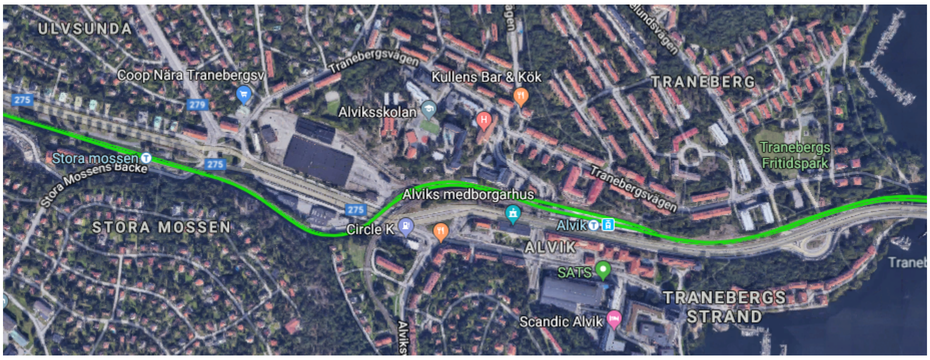

Figure 3.4: Location of chosen curves on the map, the green line of SL marked in green

Figure 3.5: Curve of radius 122 m marked in black

Figure 3.6: Curve of radius 318 m marked in black

3.2 Statistical screening

The screening analysis was performed on the green metro line based on data available on the associated cloud service, collected by the track monitoring system during a period of one year from September 23 in 2017 to September 23 in 2018. The number of squeal events per day detected on each path (the track stretch between stations) and track section (25 m long track segments) was accounted for. The data obtained for track paths included squeal events detected on both the northbound and southbound tracks and provided a general view on the curve squeal situation on the Stockholm metro. The data sampled per track section only included squeal generated from the northbound track. It was sorted into six categories of different curve radii where squeal events had been generated, see Table 3.1.

Table 3.1: Curve radius categories and the number of curves in each category on the northbound part of the green line at the Stockholm metro

	Category	Number of curves in category
1	100 - 200 m	5
2	200 - 300 m	14
3	300 - 400 m	44
4	400 - 500 m	20
5	500 - 700 m	48
6	700 - 900 m	32

The information required for the screening analysis was collected in a database, see Appendix A.2. Each curve was associated with the following information: a unique number, path name, section number, distance from the reference station (Slussen), curve radius, location inside or outside a tunnel and if high rail lubrication was applied. The number of squeal events was normalised with respect to the number of sections. This normalisation enables to compare the occurrence of squeal between curves of different radii. To investigate the difference in number of squeal events generated inside and outside tunnels or with and without high rail lubrication, the number of squeal events is divided by the total number of sections located inside and outside tunnels or with and without lubrication, respectively.

3.3 Logistic regression model

Logistic regression is a classification algorithm appropriate for binary dependent variables. The occurrence of squeal is a problem for which the outcome is indeed binary: squeal either occurs (positive class, $y = 1$) or not (negative class, $y = 0$). Mathematical description of the model is presented in the following section. The implementation was carried out in software R [37].

3.3.1 Mathematical description

Binary logistic regression is one of generalised linear models, for which the transformation that turns the expectation of the response into a linear expression is known as a link function. Having a binary output variable, y, it is desired to model a probability $p(y = 1|x)$ as a function of an independent variable x, which is an explanatory variable, or so-called predictor. The relationship between predictor and output variables is not linear, as $y \in \{0, 1\}$. However, the probability p, that $y = 1$ is transformed to obtain a linear function:

$$\begin{aligned} logit(p) &= ln\left(\frac{p}{1-p}\right) \\ &= \theta_0 + \theta_i x_i \end{aligned} \tag{3.1}$$

where θ_i are regression coefficients, x_i are predictor variables and θ_0 is an intercept term. This may be done with several possible transformations, e.g. logistic transformation or probit transformation [38]. In the current study, the logistic transformation, logit, is used as a link function. The logit of the probability p is the natural logarithm of an odds ratio, see Equation 3.1. It may take values from $-\infty$ ($p(y = 1|x) = 0$) to $+\infty$ ($p(y = 1|x) = 1$). Odds are ratios of the probability of squeal occurrence ($y = 1$) to the probability of no squeal ($y = 0$). The notation used in the chapter is introduced below:

- Data set with m examples: $\{(x^{(1)}, y^{(1)}), (x^{(2)}, y^{(2)}), ..., (x^{(m)}, y^{(m)})\}$
- A set of n-predictors
$$x \in \Big[x_0, x_1, x_2 ... x_n\Big]$$
- For an intercept term: $x_0 = 1$
- Output variable takes values: $y \in \{0, 1\}$

The estimated probability of $y = 1$ is represented by the sigmoid function g, which is the inverse of the logit [40]:

$$h_\theta(x) = g(x_i\theta_i) = \frac{1}{1 + e^{-\theta_i \cdot x_i}} \tag{3.2}$$

where θ_i are regression coefficients and x_i are predictor variables. Here, $h_\theta(x)$ outputs the probability that $y = 1$, given predictor, x, e.g. temperature parametrised by fitted coefficient θ, $(p(y = 1|x; \theta))$. Prediction whether the label is 0 or 1 using logistic regression parameters θ_i is computed for x_i using a threshold of 0.5, i.e. whenever $h_\theta(x)$ gives a probability of $y = 1$ that is ≥ 0.5, the prediction is set equal to 1. It means that predicted label is 1 whenever $\theta_0 + \theta_i x_i$ is not negative.

Regression coefficients, θ_i are chosen using the method of the maximum likelihood such that the observed outcome, y, is the most likely result based on the observed predictors, x_i. The maximum likelihood is computed for a particular choice of regression coefficients. The number of coefficients, θ_i, depends on the number of predictors and the order of the polynomial used in the logistic regression, see Equation 3.1. For the maximum product presented in Eqation 3.3, the optimal coefficients are found. This product is the so-called likelihood and may be shown as in Equation 3.4.

$$\prod_{j=1}^{m} p(y = 1|x; \theta) \cdot I(y = 1) \cdot p(y = 0|x; \theta) \cdot I(y = 0) \tag{3.3}$$

where $I(a = b)$ is 1 if $a = b$ is true, otherwise $I(a = b)$ is 0.

$$\prod_{j=1}^{m} p(y = 1|x; \theta)^y \cdot (1 - p(y = 1|x; \theta))^{(1-y)} \tag{3.4}$$

Finding the maximum likelihood corresponds to identifying the minimum cost. A cost function is introduced to assess the difference between the prediction, $h_\theta(x)$, and the actual outcome, y. Cost is mathematically explained in equation below.

$$Cost(h_\theta(x), y) = \begin{cases} -ln(h_\theta(x)), & \text{if } y = 1 \\ -ln(1 - h_\theta(x)), & \text{if } y = 0 \end{cases} \tag{3.5}$$

Equation (3.5) implies that the cost increases the larger the difference between the actual outcome and the predicted value becomes. This is depicted in Figure 3.7.

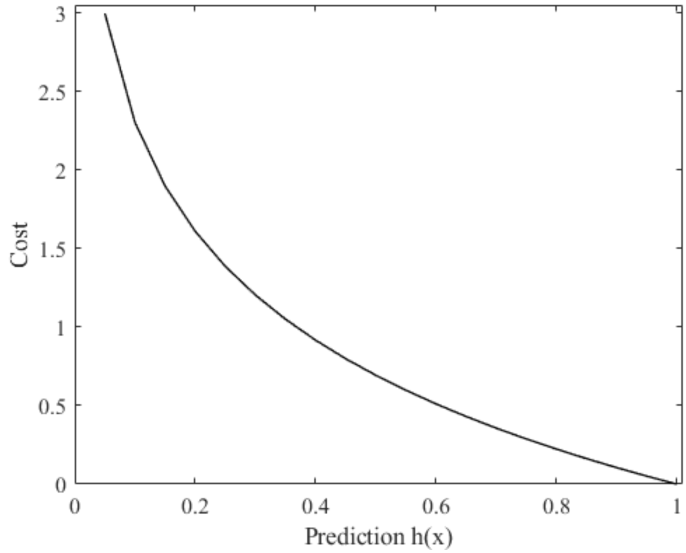

Figure 3.7: Cost as a function of predicted values $h_\theta(x)$, when $y = 1$

For the optimisation of the model parameters, the cost function may be expressed in the following form [40]:

$$\begin{aligned} J(\theta) &= -\frac{1}{m}\sum_{j=1}^{m} Cost(h_\theta(x^{(j)}), y^{(j)}) \\ &= -\frac{1}{m}\sum_{j=1}^{m}\left(y^{(j)} \cdot \ln\left(h_\theta(x^{(j)})\right) + (1 - y^{(j)}) \cdot \ln\left(1 - h_\theta(x^{(j)})\right)\right) \end{aligned} \tag{3.6}$$

where m is the number of data samples.

The concept of the cost can be extended to be used for model selection, by adding a cost that penalises explanatory variables. Logistic regression using a high order polynomial may be prone to overfitting. It occurs when the error (cost) computed based on a portion of a dataset decreases, while it simultaneously increases for another subset of the data, with increasing number of model parameters. In other words, overfitting occurs when a model fits train data set well, but fails when making predictions with new data. To avoid this, a regularisation term, that penalises parameters θ_i may be added to the cost function. The minimal cost can provide a good balance between model size and goodness of fit.

3.3.2 Model evaluation

The current study has accounted for three predictor variables (i.e. speed, humidity and temperature) and three polynomial orders were examined, i.e. 1th (model.1), 2nd (model.2) and 3rd (model.3) degree polynomial. A possible improvement of models with increasing order of polynomial was investigated using the **likelihood ratio test**. The null hypothesis that is tested, is described as follows: coefficients fitted for all terms from a higher order polynomial that do not belong to the lower order polynomial are simultaneously zero. This means that e.g. in case of the examination if model.2 is better than model.1, the hypothesis under the test claims that θ_i coefficients corresponding to parameters $X_1^2, X_2^2, X_3^2, X_1 \cdot X_2, X_1 \cdot X_3, X_2 \cdot X_3$ are $= 0$ simultaneously, see Table 3.3. The likelihood ratio test statistics as a function of two likelihoods, i.e. likelihood under the null hypothesis, L_R, and likelihood under the alternative hypothesis, L, is presented in Equation 3.7 [39]. All explanatory variables in L_R must also be in L, as L is an extension of L_R. In the test, it is calculated how much the goodness of fit is increased with the extension of the explanatory variables set. The result of $\mathscr{R}$ is then quantified with the critical limit $\chi^2_{(1-\alpha,\nu)}$ where α is the risk level and ν is the number of degrees of freedom (df), corresponding to the difference between df of both compared models. The degree of freedom is equal to the number of coefficients in the model including an intercept term, e.g. for model.1, $df = 4$. Results presented in Table 3.2 show that the model implemented with the 3rd degree polynomial (model.3) is significantly better than model.2 and model.1.

$$\begin{aligned} \mathscr{R} &= -2 \ln \left(\frac{L_R}{L} \right) \\ &= 2(\ln L - \ln L_R) \end{aligned} \tag{3.7}$$

Table 3.2: Likelihood ratio test results performed in R for model implemented with 1st, 2nd and 3rd order polynomial

	model.1 & model.2	model.2& model.3	model.1& model.3
$\mathscr{R}$	31.68	27.72	59.40
critical limit	12.59	18.31	26.30

Table 3.3: Model parameters dependent on the polynomial order

Order of polynomial	Name of the model	Parameters
1st	model.1	X_1, X_2, X_3
2nd	model.2	$X_1, X_2, X_3, X_1^2, X_2^2, X_3^2, X_1 \cdot X_2,$ $X_1 \cdot X_3, X_2 \cdot X_3,$
3rd	model.3	$X_1, X_2, X_3, X_1^2, X_2^2, X_3^2, X_1^3, X_2^3, X_3^3,$ $X_1 \cdot X_2, X_1 \cdot X_3, X_2 \cdot X_3, X_1^2 \cdot X_2,$ $X_1^2 \cdot X_3, X_2^2 \cdot X_1, X_2^2 \cdot X_3,$ $X_3^2 \cdot X_1, X_3^2 \cdot X_2, X_1 \cdot X_2 \cdot X_3$

The influence of the predictor on the outcome variables can be tested with the so-called probability value or **p-value**. A p-value is the outcome from a hypothesis test of the null hypothesis. In case of the current problem, the null hypothesis would claim, that there is no relationship between predictors (i.e. speed, humidity or temperature) and the outcome. A small p-value implies that observed data do not fit the null hypothesis. For a p-value lower than the specified significance level (usually 5 %) the null hypothesis is rejected and the result is considered statistically significant [34].

According to p-values presented in Table 3.4 -Table 3.6, results for the vehicle speed (X_1) as well as all terms that contain X_1 are greater than the significance level of 5 %. The term $X_2^2 \cdot X_3$ from the 3rd order model has the p-value of 0.824, which is also above the given threshold, see Table 3.6. The likelihood ratio test of the 3rd order model (model.3) and the model with the reduced number of explanatory variables by the mentioned insignificant predictors, shows, that the goodness of fit is decreased with the extension of the explanatory variables set, see Table 3.7 and Table 3.8. In other words, the 3rd order model with the reduced number of predictors is better than the model.3. Hence, the model with the 3rd order polynomial (model.a), including only humidity and temperature and the set of explanatory variables reduced by term $X_2^2 \cdot X_3$ was selected for the further logistic regression analysis.

Table 3.4: Coefficients, p-values and Standard Error calculated for the 1st order model with 3 predictors (speed, humidity, temperature), based on the train data set collected on the northbound track at the 122 m radius curve located between stations Alvik and Stora mossen during the time period 2017-08-25 - 2018-11-30. A detailed description of the train data set is found in Section 4.3.1

Explanatory variable	Estimated coefficient	Standard Error	p-value
Speed (X_1)	- 0.0021	0.0348	0.952
Humidity (X_2)	1.0168	0.0040	$3.18 \cdot 10^{-5}$ ***
Temperature (X_3)	-0.0027	0.0082	0.744

Table 3.5: Coefficients, p-values and Standard Error calculated for 2nd order model with 9 predictors, based on the train data set collected on the northbound track at the 122 m radius curve located between stations Alvik and Stora mossen during the time period 2017-08-25 - 2018-11-30. A detailed description of the train data set is found in Section 4.3.1

Measure	Estimated coefficient	Standard Error	p-value
Speed (X_1)	0.9801	0.8319	0.2388
Humidity (X_2)	0.0470	0.0856	0.5829
Temperature (X_3)	0.1589	0.1719	0.3552
X_1^2	-0.0167	0.0117	0.1542
X_2^2	-0.0007	0.0002	0.0010 **
X_3^2	-0.0041	0.0009	$1.4 \cdot 10^{-5}$ ***
$X_1 \cdot X_2$	0.0022	0.0022	0.3380
$X_1 \cdot X_3$	-0.0003	0.0046	0.9518
$X_2 \cdot X_3$	-0.0011	0.0006	0.0627 .

Table 3.6: Coefficients, p-values and Standard Error calculated for 3rd order model with 19 predictors, based on the train data set collected on the northbound track at the 122 m radius curve located between stations Alvik and Stora mossen during the time period 2017-08-25 - 2018-11-30. A detailed description of the train data set is found in Section 4.3.1

Measure	Estimated coefficient	Standard Error	p-value
Speed (X_1)	-9.0331	11.7370	0.4415
Humidity (X_2)	-1.5516	1.0357	0.1341
Temperature (X_3)	0.5011	2.0398	0.8059
X_1^2	0.1977	0.3236	0.5413
X_2^2	0.0054	0.0047	0.2540
X_3^2	-0.0481	0.0218	0.0270 *
X_1^3	-0.0014	0.0031	0.6452
X_2^3	-0.0000	0.0000	0.0509 .
X_3^3	0.0003	0.0001	0.0074 **
$X_1 \cdot X_2$	0.0735	0.0520	0.1578
$X_1 \cdot X_3$	0.0197	0.1080	0.8554
$X_2 \cdot X_3$	-0.0010	0.0131	0.4450
$X_1^2 \cdot X_2$	-0.0009	0.0007	0.208
$X_1^2 \cdot X_3$	-0.0004	0.0016	0.8211
$X_1 \cdot X_2^2$	-0.0001	0.0001	0.6346
$X_3 \cdot X_2^2$	0.0000	0.0000	0.4179
$X_1 \cdot X_3^2$	0.0004	0.0006	0.4422
$X_2 \cdot X_3^2$	0.0003	0.0001	0.0005 ***
$X_1 \cdot X_2 \cdot X_3$	-0.0000	0.0003	0.9215

Table 3.7: Coefficients, p-values and Standard Error calculated for the reduced 3rd order model with 8 predictors (model.a), based on the train data set collected on the northbound track at the 122 m radius curve located between stations Alvik and Stora mossen during the time period 2017-08-25 - 2018-11-30. A detailed description of the train data set is found in Section 4.3.1

Measure	Estimated coefficient	Standard Error	p-value
Humidity (X_2)	-0.2263	0.1139	0.0470 *
Temperature (X_3)	0.5661	0.1210	$2.9 \cdot 10^{-6}$ ***
X_2^2	0.0050	0.0018	0.0065 **
X_3^2	-0.0286	0.0065	$9.59 \cdot 10^{-6}$***
X_2^3	-0.0000	0.0000	0.00212 **
X_3^3	0.0002	0.0001	0.0083 **
$X_2 \cdot X_3^2$	0.0003	$6.41 \cdot 10^{-5}$	$6.87 \cdot 10^{-5}$ ***
$X_2 \cdot X_3$	-0.0064	0.0015	$1.4 \cdot 10^{-5}$ ***

Table 3.8: Likelihood ratio test results for model implemented with 3rd order polynomial with 19 predictors, including speed, humidity and temperature (model.3) and the reduced model with 3rd polynomial with 8 predictors, excluding vehicle speed (all terms including speed) and term $X_2^2 \cdot X_3$ (model.a)

	model.a & model.3
$\mathscr{R}$	7.76
critical limit	19.68

Decision boundary is a separator between classes (squeal, $y = 1$, or no squeal, $y = 0$) calculated by the developed logistic regression model. In a scatter plot the decision boundary is visualised by e.g. a line, a plane or a surface shape. In the following the concept is exemplified with a simple one degree polynomial to predict squeal using vehicle speed and humidity as predictors. A simple boundary plot may be created with the equation below:

$$h_\theta(x) = p(y = 1|x_1, x_2; \theta) = g(z) \tag{3.8}$$

$$z = \theta_0 + \theta_1 x_1 + \theta_2 x_2 \tag{3.9}$$

An example sigmoid function is presented in Figure 3.8. It is clear, that $g(z) \geq 0.5$ when $z \geq 0$.

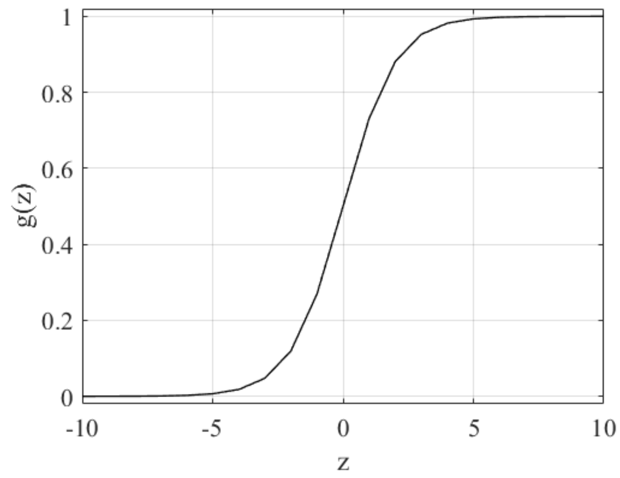

Figure 3.8: Sigmoid function of an example z

Therefore, to predict when $y = 1$, Equation 3.9 can be transformed into the following relationship:

$$\theta_0 + \theta_1 x_1 + \theta_2 x_2 \geq 0 \tag{3.10}$$

Having determined the optimal θ_i coefficients, a line that separates classes may be plotted as presented in Figure 3.9. The plot shows, that for conditions that fall above the separating line, e.g. speed of 40 km/h and humidity of 95 %, the model predicts that squeal occurs, $y = 1$. It illustrates the concept of decision boundaries on a 2D example, with only 2 predictors (x_1, x_2). The data used in this illustration is taken from 122 m radius curve between Alvik and Stora mossen on the Stockholm metro. More detailed results from this curve are found in the Results chapter.

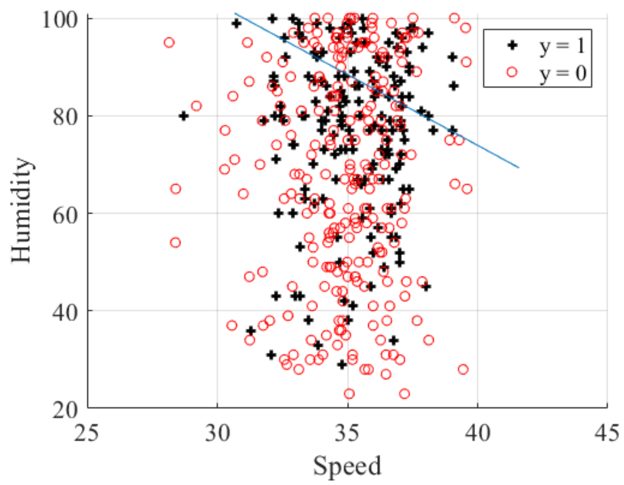

Figure 3.9: Example decision boundary plot for prediction of squeal occurrence $(y = 1)$ using 2 predictors i.e. vehicle speed and humidity (x_1, x_2) and coefficients: $\theta_0 = -4.19, \theta_1 = 0.064, \theta_2 = 0.022$

In order to assess the accuracy of the logistic regression model and the model fit, it is essential to divide a dataset into separate subsets to train and test the logistic regression model. In the current study, 70 % and 30 % of the dataset was used to train and test the logistic regression model, respectively. Evaluation of the logistic regression model is enabled by showing train data samples in a decision boundary plot to estimate how well the model fits the data. Such visualisation performed on the test dataset enables to discover overfitting which corresponds to when the model fits the train data set well, but fails to predict future data.

A few metrics to indicate how well the model fits the data may be calculated:

- **Accuracy** is a ratio between the number of correct predictions and the total number of predictions.

$$Accuracy = \frac{TP + TN}{TP + TN + FP + FN}$$

  where TP (True Positive) and TN (True Negative) corresponds to that the model correctly predicts positive and negative classes, respectively, and FP (False Positive) and FN (False Negative) corresponds to that the model incorrectly predicts positive and negative classes, respectively.

- **Precision** indicates the proportion of positive identifications that was correct. In other words, the percentage of the samples where a squeal event was correctly predicted.

$$Precision = \frac{TP}{TP + FP}$$

- **Recall** measures what proportion of actual positives was identified correctly.

$$Recall = \frac{TP}{TP + FN}$$

4

Results

In this chapter, results from the screening and logistic regression analysis of curve squeal generated on the Stockholm metro are presented and discussed. These investigations only considered squeal generated from the low wheel–rail contact. However, cases with flange noise radiated from the outer wheel during curve negotiation have also been identified. In the following, typical characteristics of the squeal noise recorded at curves selected for the logistic regression analysis are described.

4.1 Squeal noise characteristics

Noise recorded in the Quiet Track Monitoring System (QTMS) during selected passages on the northbound track in the curve between Alvik and Stora mossen, see Section 3.1.4, is used to illustrate squeal noise characteristics. A description of the QTMS is found in Section 3.1. Spectrograms for cases with curve squeal, flanging noise with less severe squeal and case without squeal or flanging noise recorded with microphone number 2 are shown in Figure 4.1 and Figure 4.2.

Curve squeal was identified using the criterion described in Section 3.1.2. Flanging noise was identified using aural perception and description found in the literature, e.g. [10]. In case with flanging noise, the noise measured with microphone 2 exceeds that of measured with microphone 1, see Figure 4.3 and Figure 4.4. It is assumed that microphone number 2 is in this case located near the high wheel. There is no such difference observed in the sound pressure for the case that squeal is not generated, see Figure 4.5. Recordings were done on three days in October 2017. Detailed information about time, vehicle speed and weather conditions are included in Appendix A.1.

The rolling noise has a broadband frequency content contained in lower and low-mid frequency range below 1 kHz, with a significant frequency component at approximately 600 Hz and its harmonics. Figure 4.2 shows the noise level measured for the case without squeal to be significantly lower compared to passages with squeal, especially above 3.2 kHz. This difference is equivalent to approximately 6 dBA.

Passages with squeal are characterised by tonal components and higher harmonics. The squealing frequency is at 1030 Hz. The maximum noise levels are measured for curve squeal at 6.2 kHz. For the passage with flanging noise and less severe curve squeal, as strong maxima in sound pressure level around harmonics frequencies are not observed. Compared to curve squeal, flanging noise is noticed to be associated with increased levels of noise in the high-frequency range above 6 kHz, see Figure 4.2. Apart from this, peaks in noise levels measured for both passages with squeal present coincide in terms of frequency. These results illustrate curve squeal generated at the same curve and by the same vehicle with similar frequency characteristic for different passages. The absence of tonal components related to squeal in the noise recorded for the passage without squeal generation is noticed in Figure 4.1 and Figure 4.2.

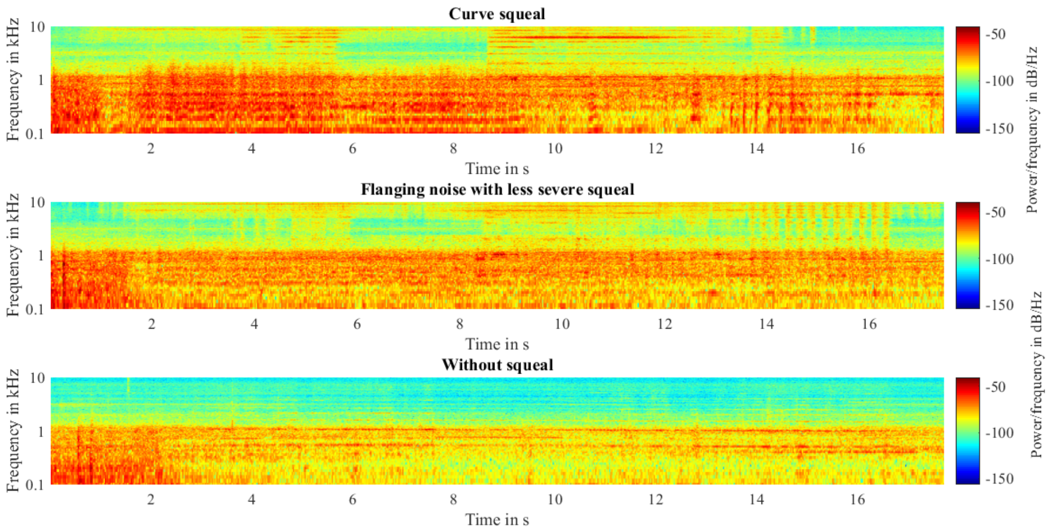

Figure 4.1: Spectrogram of noise measured during three different passages through the 122 m radius curve between Alvik and Stora mossen

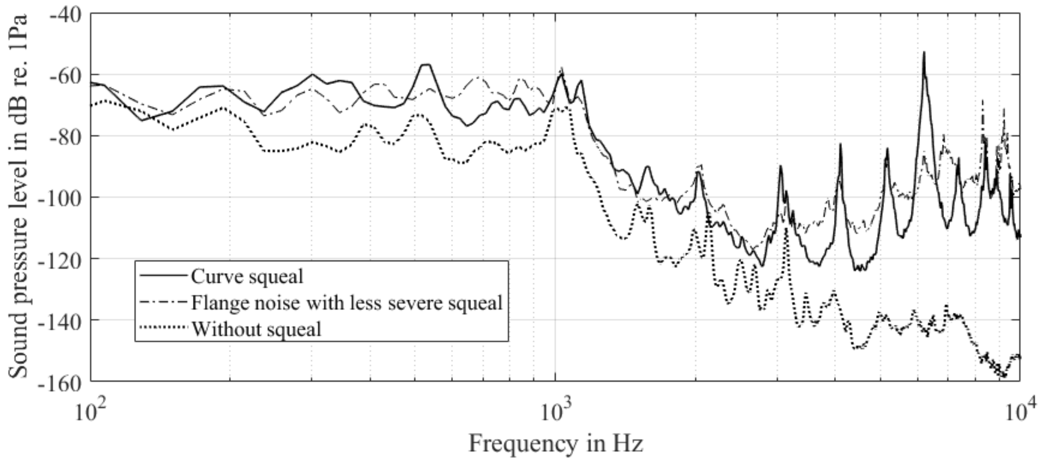

Figure 4.2: Spectra of noise measured during three different passages through the 122 m radius curve between Alvik and Stora mossen

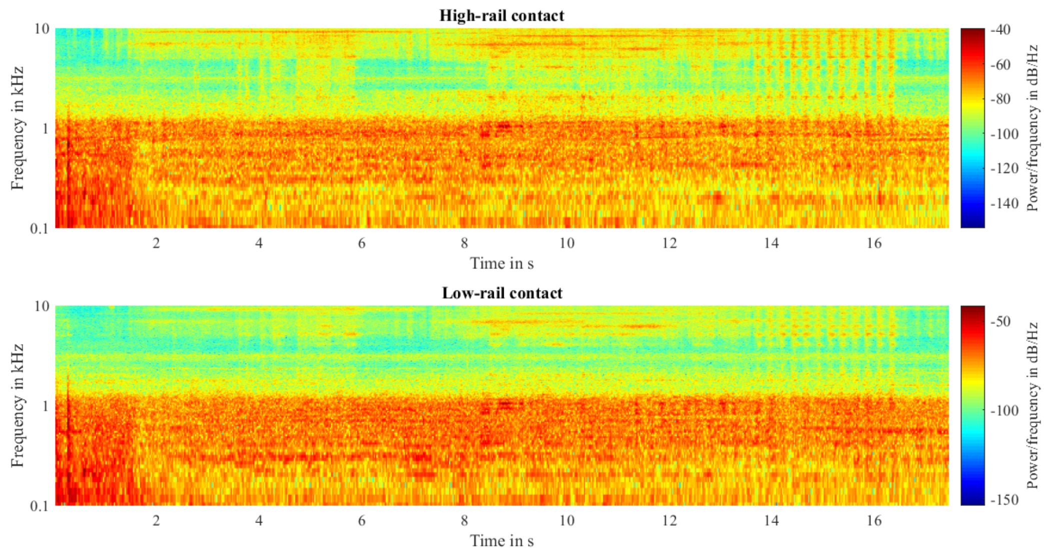

Figure 4.3: Spectrogram of noise identified as flanging noise with less severe squeal, measured during a passage through the 122m radius curve between Alvik and Stora mossen

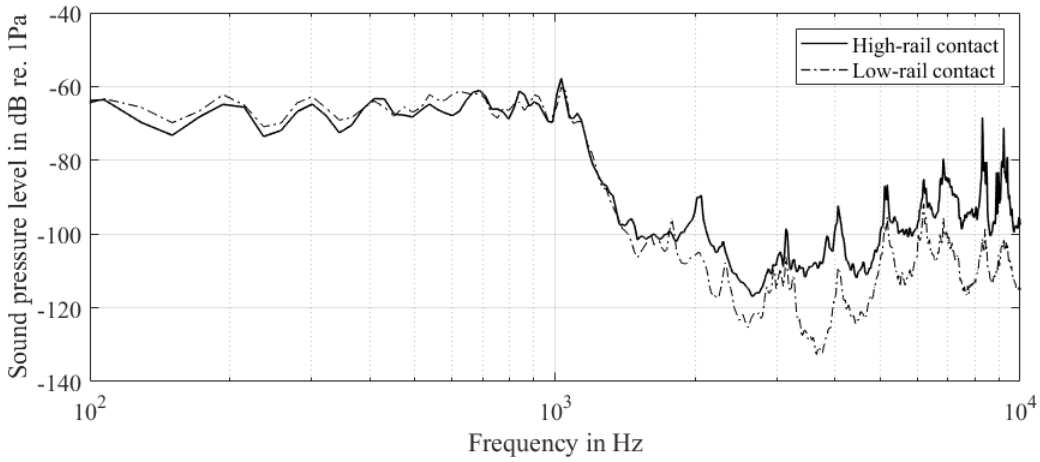

Figure 4.4: Spectra of noise identified as flanging noise with less severe squeal, measured during a passage through the 122 m radius curve between Alvik and Stora mossen

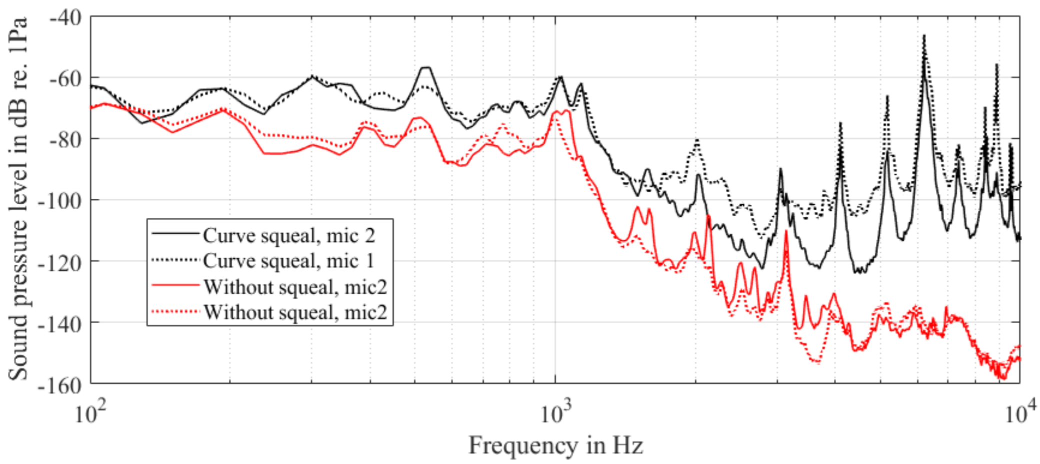

Figure 4.5: Spectra of noise measured during 2 different passages through the 122 m radius curve between Alvik and Stora mossen

Additionally, spectra of noise recorded with microphone number 2 at three different curves: two located between stations Alvik and Stora mossen, with the radius of 122 m and 318 m, and one located between stations Gullmarsplan and Skärmarbrink with radius 150 m were compared. Detailed information about time, vehicle speed and weather conditions are included in Appendix A.1. For all three passages squeal occurs and noise spectra shows that squealing frequency as well as its harmonics patterns coincide, see Figure 4.7. These results illustrate curve squeal generated by the same vehicle with identical frequency characteristic at different curves.

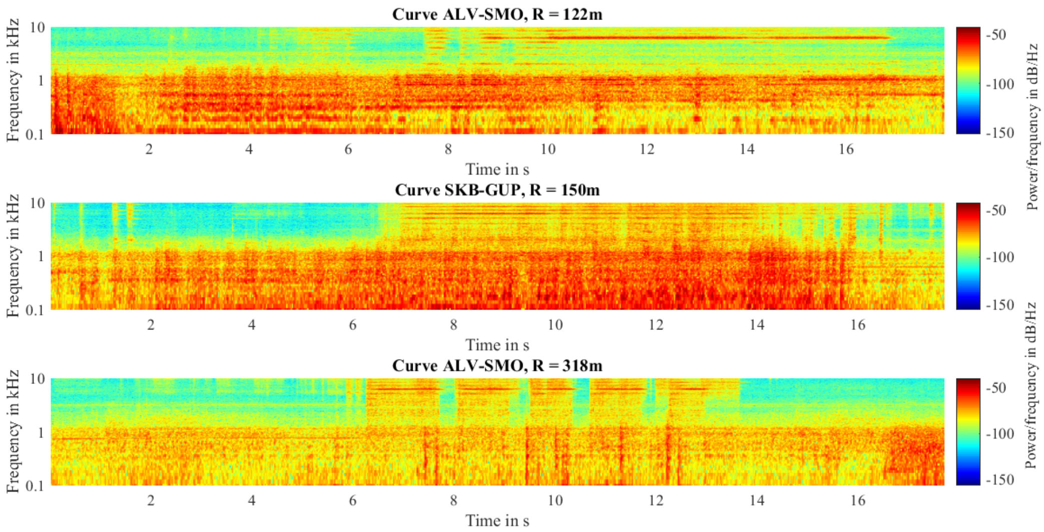

Figure 4.6: Spectrogram of noise measured during three different passages through the three different curves on the green line of SL

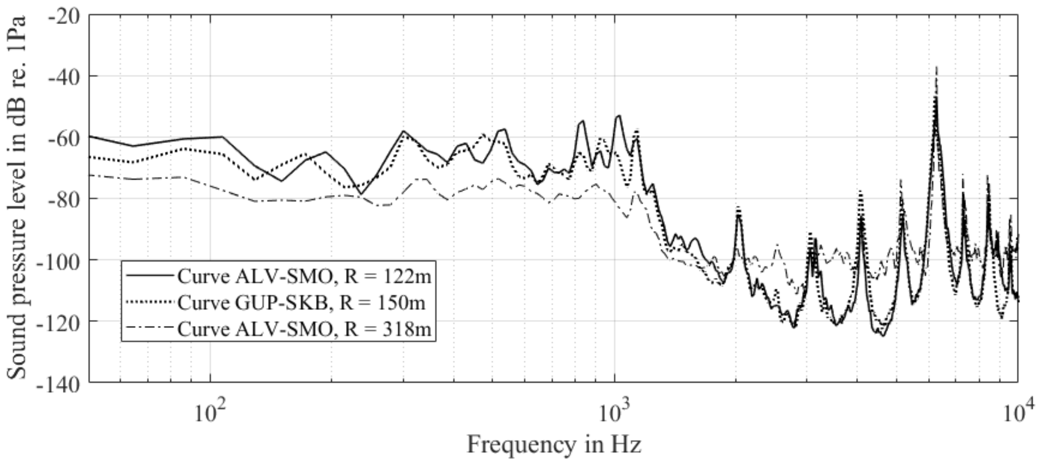

Figure 4.7: Spectra of noise measured during three different passages through the three different curves on the green line of SL

4.2 Screening analysis

A screening analysis was performed based on data collected on the green metro line by the QTMS containing number of squeal events per day detected using the criterion described in Section 3.1.2. Results presented in this section were obtained with data collected during a period of one year from September 23 in 2017 to September 23 in 2018. The data obtained for track paths (the track stretch between stations) included squeal events detected on both the northbound and southbound tracks. The data sampled per track section (25 m long track segments) only included squeal generated from the northbound track. Documentation of track alignment included information about the location of curves in meters from reference station Slusen, curve radius, vehicle speed limit, location inside or outside the tunnel and the distance from the reference station, at which possible lubrication is applied.

Figure 4.8 presents the sum of squeal events for paths on the green metro line that were most exposed to squeal during the studied period. Paths are ordered in descending number of squeal events. The path, where the largest number of squeal events were captured is located between stations Alvik and Stora mossen. It includes 4 curves with radii 113 m, 122 m, 244 m and 318 m (northbound track). The whole path is located outside the tunnel. The speed limit on track segments in curves is typically around 40-45 km/h and on straight parts in the range 60-70 km/h. The path with the second largest number of squeal events is located inside the tunnel, between stations Gamla stan and T-Centralen. The speed limit is 55 km/h at segments containing curves with smaller radii (e.g. 198 m and 203 m on the southbound track) and 60-70 km/h at straight segments and curves with larger radii (above approximately 600 m). The path located outside the tunnel between stations Gullmarsplan and Skärmarbrink is also noticed to be exposed to a large number of squeal events. The path includes curves with radius between 150 m - 500 m. At the curve with radius 150 m, the vehicle speed is limited to 30 km/h. The path between stations T-Centralen and Hötorget (HÖT-TCT) contains a curve with radius 213 m and speed limit 55 km/h. The path is located inside the tunnel. The path exposed to fifth largest number of squeal events during the studied period is located inside the tunnel between stations Fridhemsplan and S:t Eriksplan in the northbound direction. On segments that include curves with radii 265 m and 369 m, the speed limit is 55 km/h, on other parts of this path, the speed limit reaches 70 km/h.

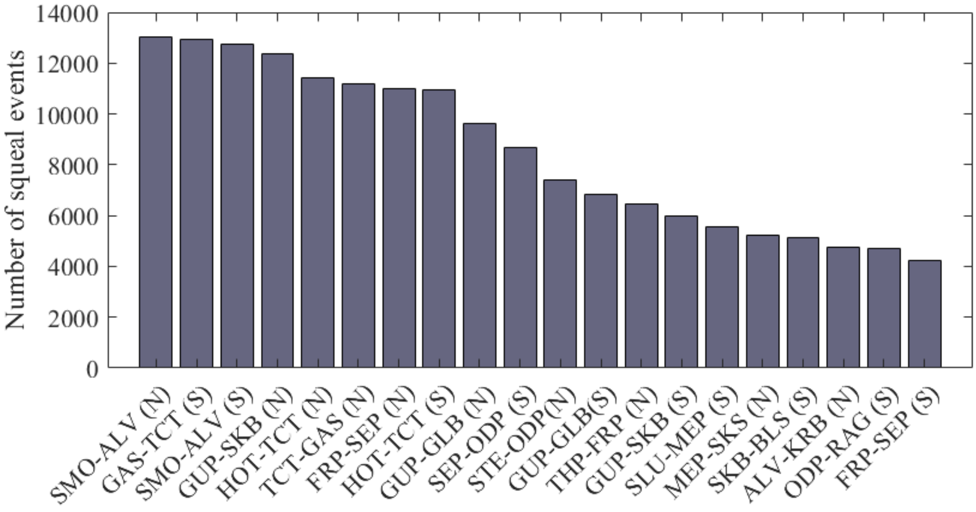

Figure 4.8: Sum of squeal events for track paths on the green metro line of SL that were most exposed to squeal during the period 2017-09-23 - 2018-09-23. (N) northbound track, (S) southbound track

The number of squeal events generated in several curves is summed into curve radius categories. A more detailed description is found in Section 3.2 and Table 3.1. The number of squeal events as a function of the curve radius category is presented in Figure 4.9. The number of squeal events measured during the studied period was divided by the number of sections. This is referred to as normalised number of squeal events. The influence of curve radius on curve squeal is obvious; the number of normalised squeal events is seen to increase with decreasing curve radius.

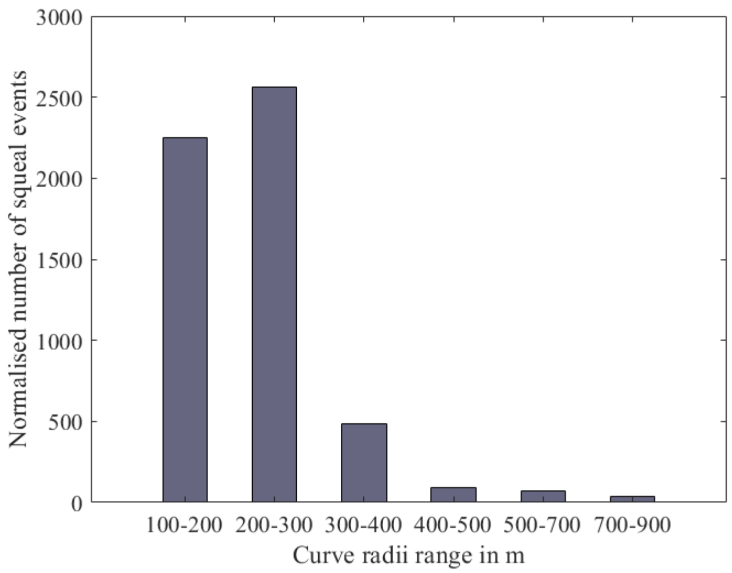

Figure 4.9: Normalised number of squeal events on the green metro line measured during the period 2017-09-23 - 2018-09-23. Squeal events generated in different curves are summed into curve radius categories, see Table 3.1

Figure 4.10 presents the normalised number of squeal events for curves that belong to the different curve radius categories separately. For all curve radius categories apart from 100-200 m and 200-300 m (containing a number of 5 and 14 curves, respectively), results are shown for the 15 curves with the maximum number of squeal events. The numbering of curves are according to the documentation, see Appendix A.2. The maximum number of squeal events are noticed to occur for curves 1 and 6 in curve radius category 200-300 m. It needs to be emphasised, that curves number 1, 2 ,3, 4, 9, 11 and 12 have radii between 200 m-222 m. The curve number 6, that is the most exposed to squeal, has the radius of 244 m and is located in vicinity of curve number 1 in curve radius category 1. These curves are located between stations Alvik and Stora Mossen.

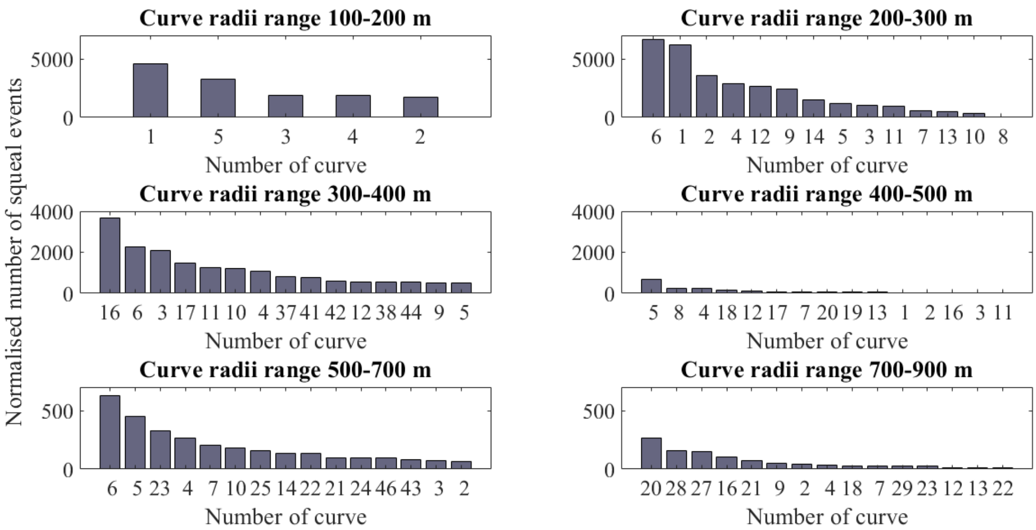

Figure 4.10: Normalised number of squeal events on the green metro line measured during the period 2017-09-23 - 2018-09-23. Results are presented for curves that belong to the different curve radius categories separately, see Table 3.1. For more information regarding the numbering of the curves see the documentation in Appendix A.2.

In the literature study of Section 2.2.4 a criterion is described that specifies curve squeal not to occur when the ratio between the curve radius and the bogie wheelbase is greater than 100 [4]. The bogie wheelbase for the Bombardier C20 metro train is 2.3 m, which implies that curve squeal should not occur for curve radius that exceeds 230 m. From Figure 4.10, the number of squeal events was noticed to reduce significantly for curves with radii larger than 222 m. Figure 4.11 shows that, although less frequent, curve squeal still occurs above the estimated threshold. In fact, it was observed that squeal is consistently not generated on curves with radius that exceeds 900 m.

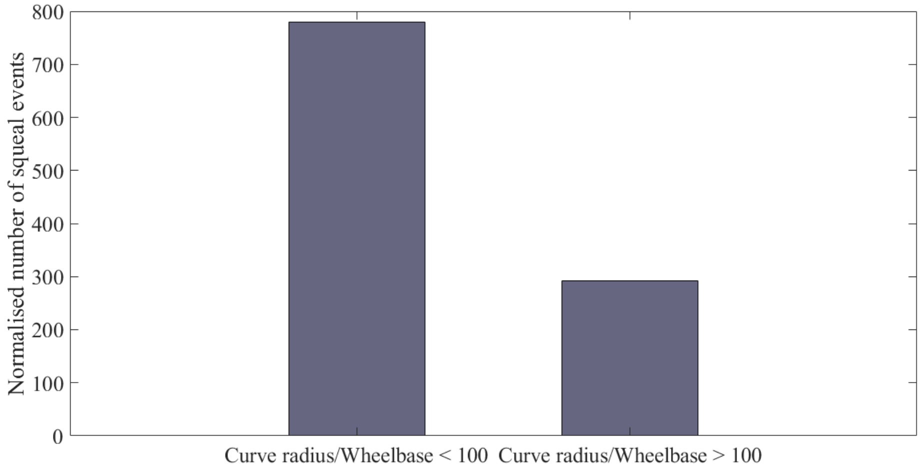

Figure 4.11: Normalised number of squeal events on the green metro line measured during the period 2017-09-23 - 2018-09-23 and categorised according to the criterion described in [4] that specifies that curve squeal should not occur for cases when the ratio between curve radius and bogie wheelbase is larger than 100.

The influence of meteorological conditions on the occurrence of curve squeal is investigated. The meteorological data was obtained from the webpage of Swedish Meteorological and Hydrological Institute (SMHI) [36]. Data contains mean day temperature measured at meteorological station Stockholm A and sum of day precipitation measured at station Stockholm.

Figure 4.12 compares the total number of squeal events captured each day on the green metro line during the studied time period against the precipitation. The corresponding figure showing the total number of squeal events against the temperature is found in Appendix A.3, see Figure A.19. The total number of squeal events captured each day on the green metro line during the studied time period presented for the different curve radius categories separately is found in Appendix A.3, see Figure A.20. The generation of squeal seems moderate in October, November and August. Squeal occurrence seems to be reduced during precipitation. The sum of squeal events detected on days with no precipitation was 1224.6/day and 861.5/day for days with precipitation. This agrees with e.g. results from in-situ test in dry/wet conditions indicating that curve squeal was eliminated after the rail was water sprayed, see Figure 2.11 [25].

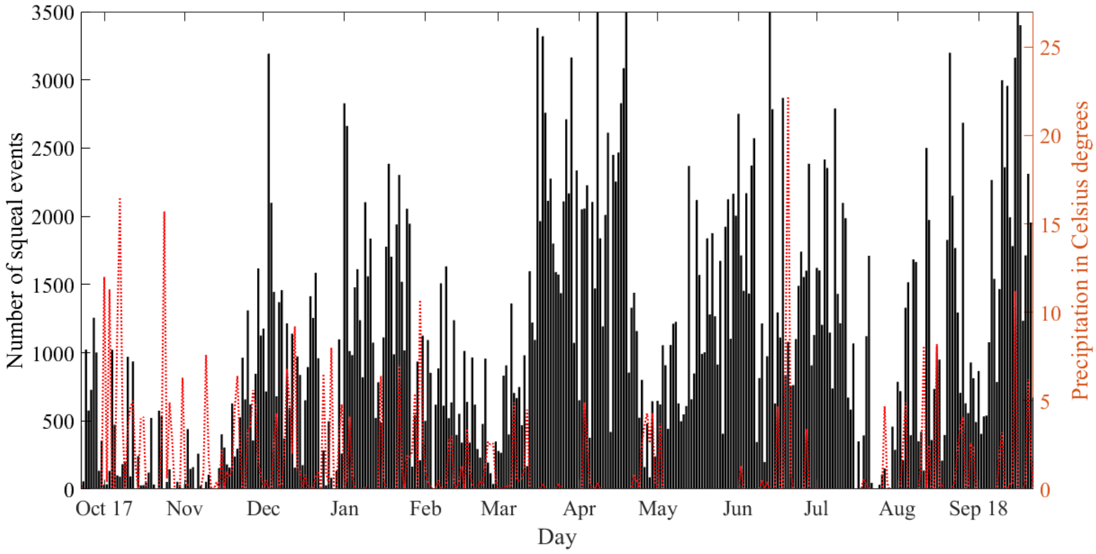

Figure 4.12: Comparison between number of squeal events per day on the green metro line measured during period 2017-09-23 - 2018-09-23 and the sum of day precipitation

To reduce wear on the gauge face of high rails, lubrication is applied on several curves at SL. The potential influence of rail lubrication and curve location (inside or outside of tunnels) on curve squeal is investigated in Figure 4.14 and Figure 4.13, respectively. Squeal events are normalised with respect to the number of sections located inside or outside of tunnels and with and without lubrication applied, respectively. It should be noted that the influence of precipitation on the occurrence of curve squeal generated outside of tunnels might be contained in the results presented in Figure 4.14. Figure 4.13 does not indicate high rail lubrication to have a significant influence on generation of curve squeal. It must be emphasised, that lubrication is usually applied at curves with smaller radius, that are the most exposed to wear and also squeal. Therefore, the increased number of squeal events generated at curves with high–rail lubrication applied may be seen.

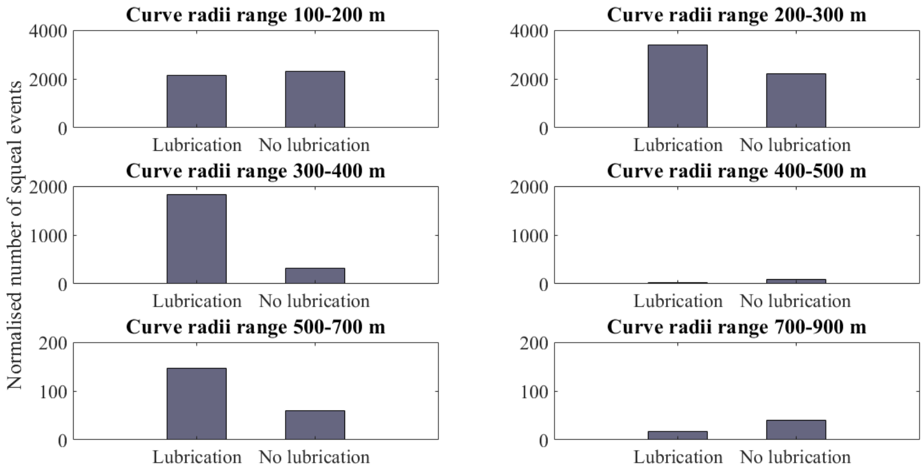

Figure 4.13: Normalised number of squeal events on the green metro line measured during the period 2017-09-23 - 2018-09-23. Comparison between curves with and without high rail lubrication

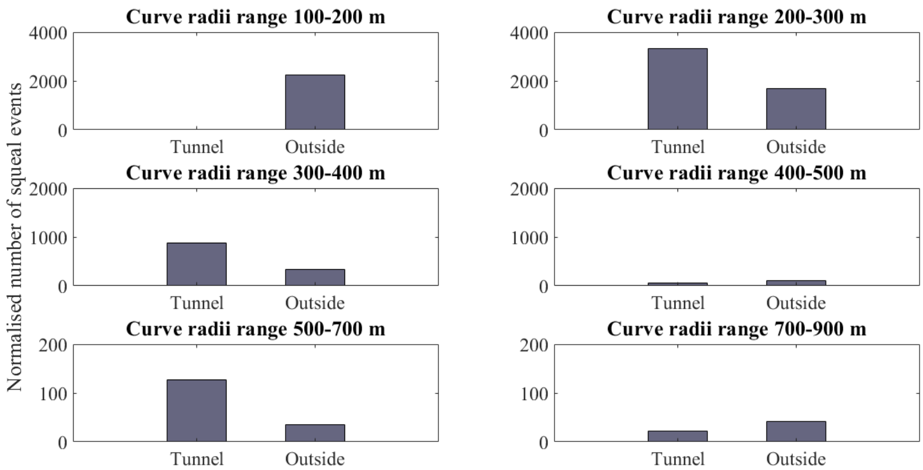

Figure 4.14: Normalised number of squeal events on the green metro line measured during the period 2017-09-23 - 2018-09-23. Comparison between curves located inside and outside of tunnels

4.3 Logistic regression analysis

In this section results obtained by logistic regression analysis are presented. Two curves of radii 122 m and 318 m located on the northbound track between stations Alvik and Stora Mossen are considered, see Figure 3.4.

4.3.1 Description of data

The data used in the logistic regression analysis of the 122 m radius curve are summarised in Table 4.1 and Table 4.2 as well as in Figure 4.15 - Figure 4.16. The corresponding results obtained for the 318 m radius curve are found in Appendix A.4. The train and test data sets include 990 (410 positive and 580 negative) and 425 (169 positive and 256 negative) samples, respectively, collected during the period 2017-08-25 - 2018-11-30. Positive samples correspond to passages for which squeal was detected, in case of negative samples, squeal was not identified. The criterion used to detect squeal is described in Section 3.1.2. Details about the location of the curve, traffic conditions and track alignment at the site are found in Section 3.1.4. From Figure 4.15, a potential relation between curve squeal and humidity is noticed. The train and test data sets are similar to each other (concurrently, data samples that are in the train data set are not included in the test data set). The train data set as dependent on the 2 predictors, humidity and temperature, is presented as scatter plot in Figure 4.17.

The logistic regression model was created with threshold 0.5, see Section 3.3.1.

Table 4.1: Summary of predictors. Train data set collected on the northbound track at the 122 m radius curve located between stations Alvik and Stora mossen during the period 2017-08-25 - 2018-11-30

Parameter	Humidity	Temperature
Unit	%	^{o}C
Min	21	-13.5
Max	100	30.6
Median	76	8.4
Mean	71.48	9.22
Standard deviation	20.29	9.81

Table 4.2: Summary of predictors. Test data set collected on the northbound track at the 122 m radius curve located between stations Alvik and Stora mossen during the period 2017-08-25 - 2018-11-30

Parameter	Humidity	Temperature
Unit	%	^{o}C
Min	23	-10
Max	100	30.6
Median	74	10
Mean	71.25	9.80
Standard deviation	21.02	9.34

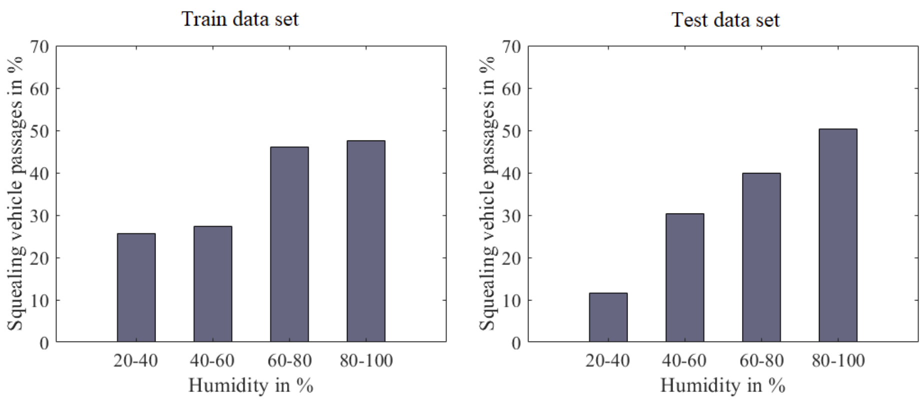

Figure 4.15: Percentage squealing passages as a function of relative humidity. Train and test data sets collected on the northbound track at the 122 m radius curve located between stations Alvik and Stora mossen during the period 2017-08-25 - 2018-11-30

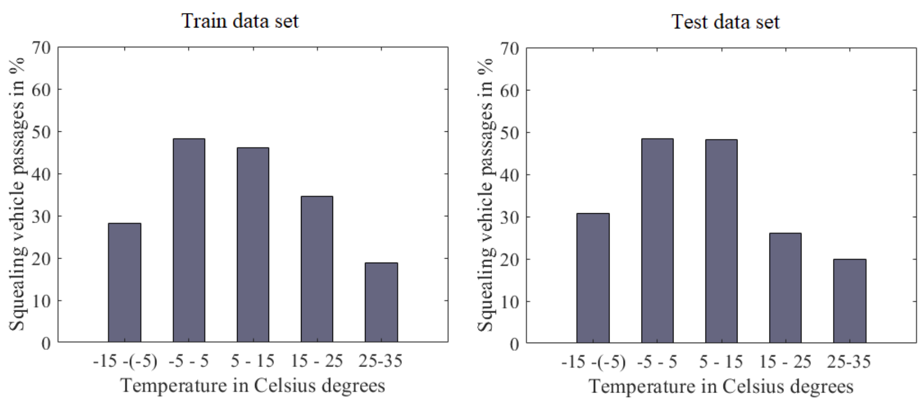

Figure 4.16: Percentage squealing passages as a function of temperature. Train and test data sets collected on the northbound track at the 122 m radius curve located between stations Alvik and Stora mossen during the period 2017-08-25 - 2018-11-30

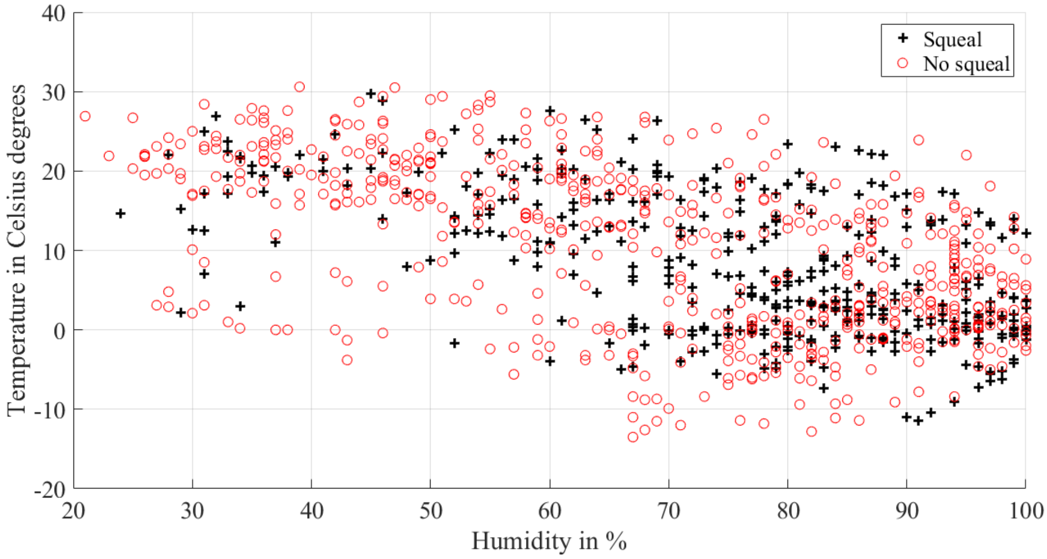

Figure 4.17: Train data set collected on the northbound track at the 122 m radius curve located between stations Alvik and Stora mossen during the period 2017-08-25 - 2018-11-30

4.3.2 Evaluation of the model

In the logistic regression, probability of squeal is modelled using 8 parameters, i.e. humidity (X_2), temperature (X_3), etc., as described in Section 3.3.1. For the implementation of the logistic regression model, software R was used. Exponents of logistic regression coefficients, θ_i are odds ratios. The list of all 9 logistic regression coefficients and their exponents including intercept term, θ_0 is presented in Appendix A.5. According to Table A.7, an increase of humidity (X_2) by 1 % contributes to drop of the probability of squeal by a factor of 1.077 while other explanatory variables are constant and an increase of temperature by 1^oC contributes to growth of the probability of squeal by a factor of 1.36 while other explanatory variables are constant. The list of all 9 exponents of coefficients estimated for 318 m radius curve, including the intercept term, θ_0 is presented in Appendix A.5.

In Table 4.3, the accuracy, precision and recall of the models for the 122 m and 318 m radius curves are summarised. The train and test accuracy are evaluated on the train and test data sets, respectively. The test accuracy of approximately 60 % indicates that the prediction of curve squeal based on the chosen predictors performs slightly better than a chance that would correspond to the accuracy of 50 %. According to the precision for the 122 m and 318 m radius curves, the models are approximately 47 % and 62 %, respectively, correct when predicting that squeal occurs ($y = 1$), see Table 4.3. The recall implies what proportion of actual positives was identified correctly. According to Table 4.3, for the 122 m and 318 m radius curves 38 % and 67 % of the squeal events were correctly identified, respectively. This distinction may be due to the difference in proportion of squealing passages between studied curves, see Section 4.3.1 and Appendix A.4.

Table 4.3: Evaluation of the model fit of the two models for the 122 m and 318 m radius curves located between stations Alvik and Stora mossen. Based on data measured during the time period 2017-08-25 - 2018-11-30

Measure	Curve 122m	Curve 318m
Train accuracy	61.31 %	62.75%
Test accuracy	58.12 %	58.94%
Precision	46.72%	62.07%
Recall	0.38	0.67

Figure 4.18 represents the decision boundary plot, created for the 122 m radius curve. The boundary is indicated by the contour at probability of squeal 0.5, that separates areas of predictions, e.g. for conditions with humidity 76 % and temperature 10^oC, a point on the scatter plot is "inside" the contour and predicted label would be 1 (squeal). The decision boundary plot for the 318 m radius curve is presented in Figure 4.20. It is noticeable, that data points of positive as well as negative labels are spread over both separated areas for both models, but with a

larger number of negative labels outside the boundary. Figure 4.19 and Figure 4.21 are another representation of the logistic regression analysis results for curves with radius 122 m and 318 m, respectively. The grid depicted with green circles of different size indicates the probability of squeal, i.e. the larger the circle size, the greater estimated probability is for the given humidity and temperature conditions.

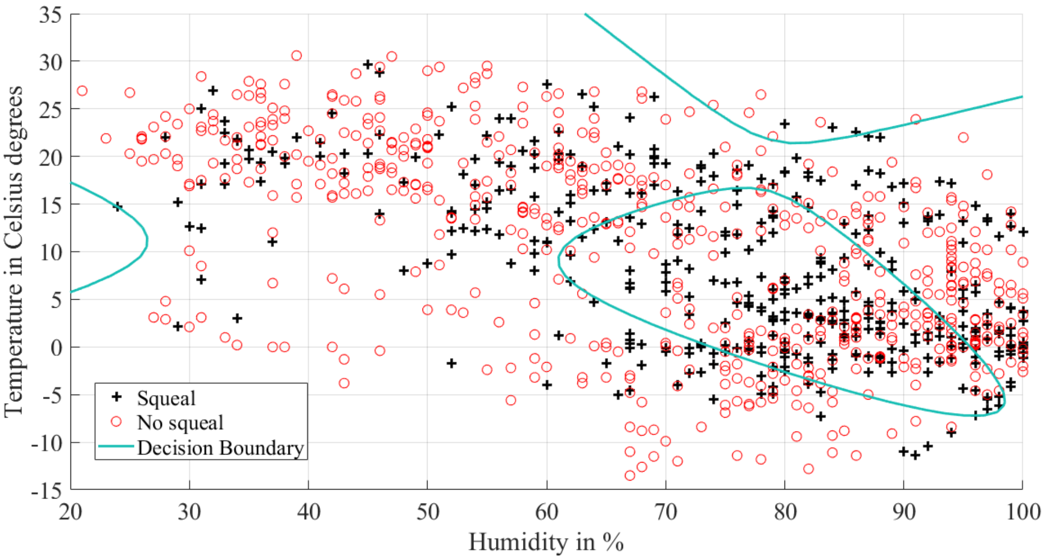

Figure 4.18: Decision boundary plot obtained with the logistic regression model developed for the train data set collected on the northbound track at the 122 m radius curve located between stations Alvik and Stora mossen during the time period 2017-08-25 - 2018-11-30. Train data samples presented

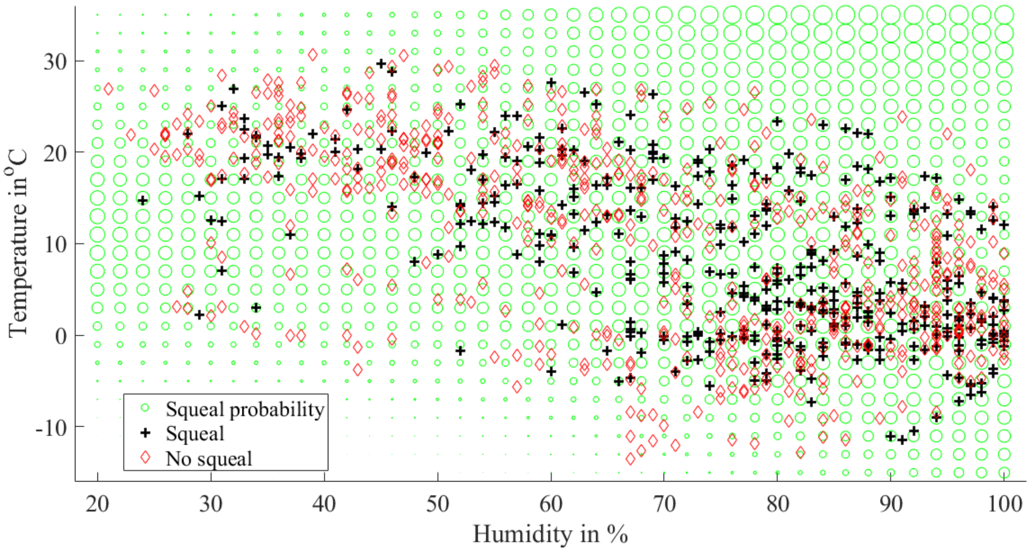

Figure 4.19: Scatter plot with a grid that indicates probability of squeal (green circles) obtained with the logistic regression model developed for the train data set collected on the northbound track at the 122 m radius curve located between stations Alvik and Stora mossen during the time period 2017-08-25 - 2018-11-30. Train data samples presented

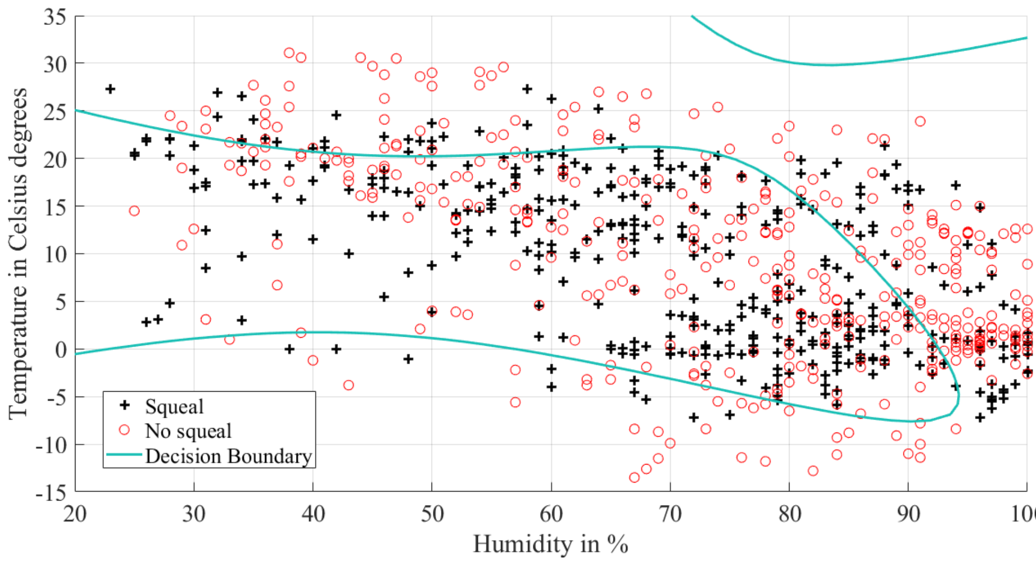

Figure 4.20: Decision boundary plot obtained with the logistic regression model developed for the train data set collected on the northbound track at the 318 m radius curve located between stations Alvik and Stora mossen during the time period 2017-08-25 - 2018-11-30. Train data samples presented

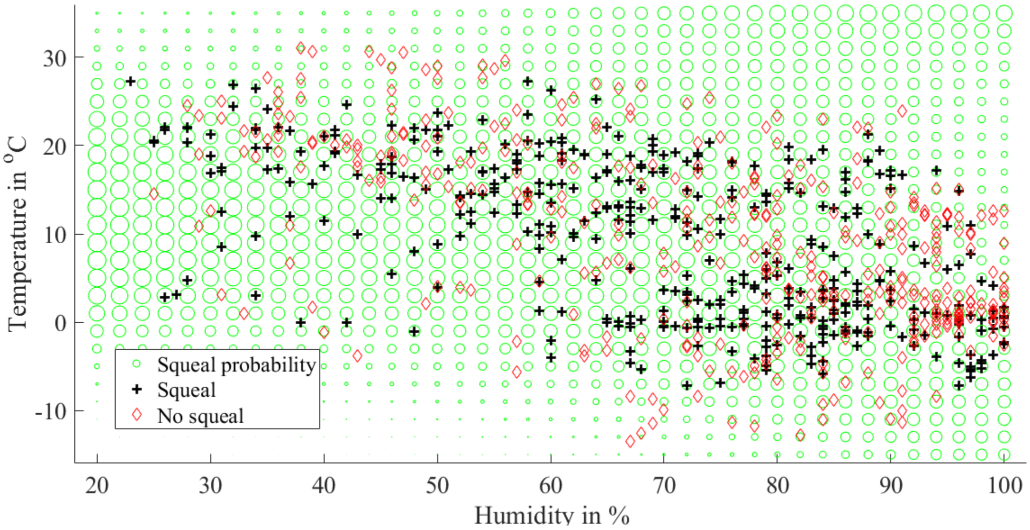

Figure 4.21: Scatter plot with a grid that indicates probability of squeal (green circles) obtained with the logistic regression model developed for the train data set collected on the northbound track at the 318 m radius curve located between stations Alvik and Stora mossen during the time period 2017-08-25 - 2018-11-30. Train data samples presented

According to Figure 4.19, humidity seems to have an influence on squeal generation. The modelled relation between humidity and squeal occurrence is presented for three different air temperatures in Figure 4.22. This trend, although as seen in Figure 4.22 dependent on temperature, is similar to that found in the results obtained on the test rig and by field test presented in [26], at humidity values of the range between 40 % - 80 %, see Figure 4.23. The corresponding results obtained with the full data set collected on the northbound track at the 122 m radius curve located between stations Alvik and Stora mossen during the time period 2017-08-25 - 2018-11-30 is presented in Figure 4.24. Similar relation between humidity and squeal occurrence or estimated squeal probability is not observed for the data measured on the 318 m radius curve, see Figure A.25-Figure A.26 in Appendix A.6.

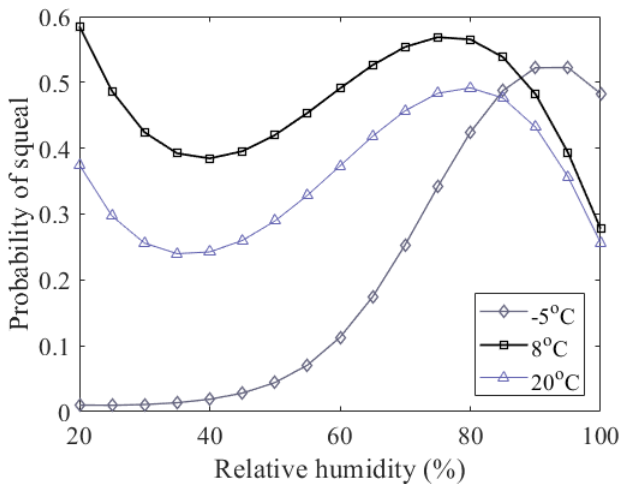

Figure 4.22: The modelled influence of relative humidity on curve squeal probability for three air temperatures. Results obtained with the logistic regression model developed for the train data set collected on the northbound track at the 122 m radius curve located between stations Alvik and Stora mossen during the time period 2017-08-25 - 2018-11-30

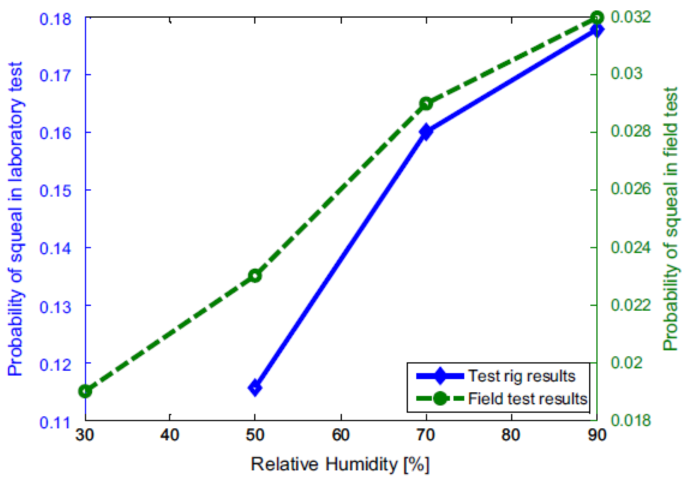

Figure 4.23: Probability of squeal in varying relative humidity [26]

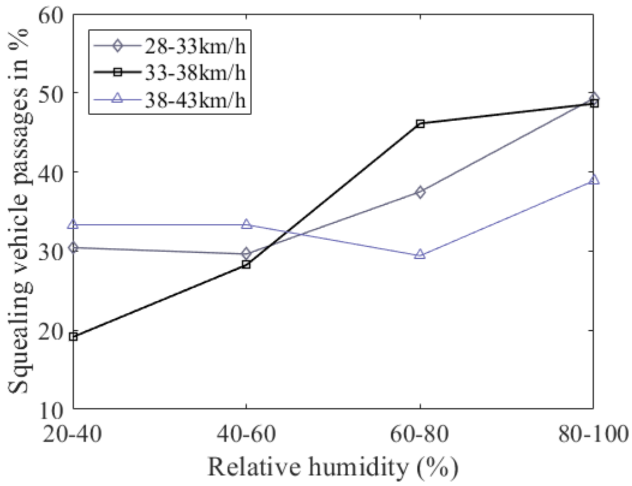

Figure 4.24: The influence of relative humidity for three different speed ranges. Full data set measured on the northbound track at the 122 m radius curve located between stations Alvik and Stora mossen during the time period 2017-08-25 - 2018-11-30

4.3.3 Further discussion

The results of the logistic regression analysis with the selected model reveal, that the model does not necessarily give predictions that are consistent with the measurement data and that the function used in the model might cause unexpected behaviour for some humidity and temperature conditions. This is for example seen in Figure 4.22, Figure 4.18 and Figure 4.19. From Figure 4.19, a few relevant observations may be emphasised:

- Few observations and very low estimated squeal probability in the left low corner, for temperature values below 16^{o}C and relative humidity below 50 %. The estimated probability of squeal drops to practically 0 for temperatures below -10^{o}C and relative humidity below 50 %

- Almost no observations and very high estimated squeal probability at top right corner. Estimated probability of squeal reaches around 0.97 for humidity around 100 % and temperature above 30^{o}C.

- Significant number of observations in the left upper corner. Here, it is observed that for humidity between 30 %-50 % and temperature in the range 17^{o}C-28^{o}C most passages did not squeal. The estimated probability of squeal in this region is between approximately 0.2 and 0.4.

- Significant number of observations in the right mid-lower corner, for temperatures below 18^{o}C and humidity above 70 %. For these conditions, it seems that most of the observations are positive, which means that most of passages squealed. Here, the estimated probability of curve squeal is between approximately 0.4 and 0.56.

The function used in the logistic regression for the current study may perform well, but only for conditions for which there were many observations. However, the function is not penalised for an uncontrolled behaviour in regions, where there are no or few observations. It may be seen as overfitting. Hence, the results from the logistic regression are only reliable in regions where there are many observations and are not recommended to be used outside these regions.

The behaviour of the model can be controlled by using a different function. Hence, the model with 5 explanatory variables, i.e. $X_2, X_3, X_2^2, X_3^2, X_2{\cdot}X_3$ was implemented. The list of coefficients and odds ratios calculated for this model is presented in Table A.8 in Appendix A.5. The comparison of the train and test accuracy of both models, i.e. the initially selected (model.a) and the reduced one (model.b) is presented in Table 4.4. Here, the possible improvement of the model fit by reducing the number of predictors is not seen or may be interpreted as ambiguous. The likelihood ratio test result indicates that the model with fewer predictors has a worse fit than the initially selected model, see Table 4.5. However, according to the estimated coefficients for humidity and the representation in Figure 4.25, the results obtained with model.b have a physical meaning that is closer to what is expected from the measurement data, see Figure 4.24. In case of model.b, the odds ratio for humidity is 1.13, which means that an increase of humidity (X_2) by 1 % contributes to an increase of the probability of squeal by a factor of 1.13 while other explanatory variables are constant. The relation between the temperature and curve squeal is presented in Figure 4.26. This shows an increase percentage of squealing passages and squeal probability at moderate temperatures, especially between 4^oC to 16^oC both for the measured and modelled data (model.b). A similar relation is shown for the 318 m radius curve, see Figure A.27 in Appendix A.6. The decision boundary plot and the plot with the grid indicating squeal probability for the 122 m radius curve, model.b are presented in Figures 4.27-Figure 4.28. Corresponding results for the 318 m radius curve are presented in Appendix A.6, see Figure A.23-Figure A.24.

Table 4.4: Evaluation of the model fit for the two logistic regression models representing the 122 m radius curve located between stations Alvik and Stora mossen. Data measured during the time period 2017-08-25 - 2018-11-30

Measure	model.a	model.b
Train accuracy	61.31 %	60.2%
Test accuracy	58.12 %	59.29%

Table 4.5: Likelihood ratio test results for the logistic regression model implemented with the reduced 3rd order polynomial, including 8 explanatory variables (model.a) respective 5 explanatory variables (model.b)

	model.b& model.a
$\mathscr{R}$	20.38
critical limit	7.81

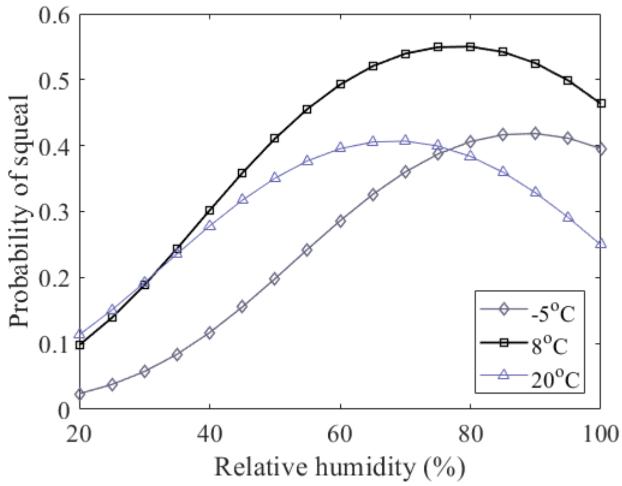

Figure 4.25: The modelled influence of relative humidity on curve squeal probability for three different air temperatures, obtained with the logistic regression model developed for the train data set collected on the northbound track at the 122 m radius curve located between stations Alvik and Stora mossen during the time period 2017-08-25 - 2018-11-30 (model.b)

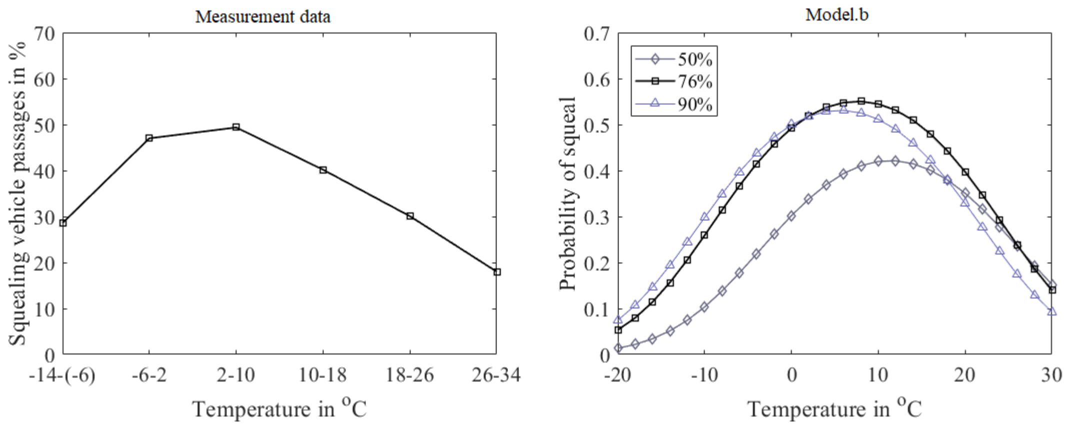

Figure 4.26: The measured relation between the air temperature and squeal occurrence based on the full data set and modelled relation between the air temperature and squeal probability for three different relative humidity values obtained with the logistic regression model developed for the train data set collected on the northbound track at the 122 m radius curve located between stations Alvik and Stora mossen during the time period 2017-08-25 - 2018-11-30

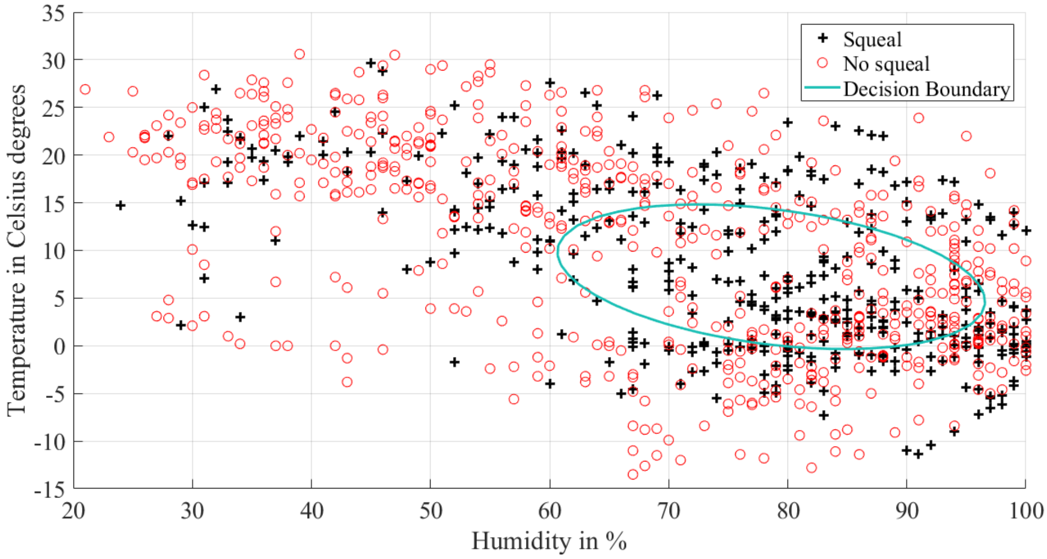

Figure 4.27: Decision boundary plot obtained with the logistic regression model developed for the train data set collected on the northbound track at the 122 m radius curve located between stations Alvik and Stora mossen during the time period 2017-08-25 - 2018-11-30. Train data samples presented (model.b)

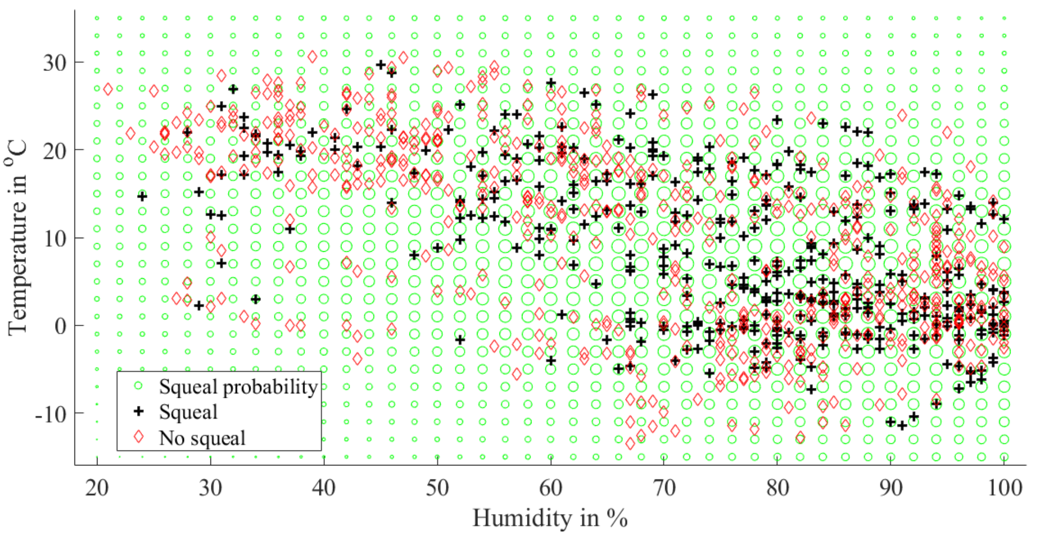

Figure 4.28: Scatter plot with a grid that indicates probability of squeal (green circles) obtained with the logistic regression model developed for the train data set collected on the northbound track at the 122 m radius curve located between stations Alvik and Stora mossen during the time period 2017-08-25 - 2018-11-30. Train data samples presented (model.b)

5

Conclusion

In this work the influence of selected variables on the generation of curve squeal has been investigated by the statistical analysis performed in two steps; (1) a screening analysis accounting for an entire metro line and (2) a detailed analysis of the conditions that promote squeal generation at two selected short radius curves exposed to severe curve squeal. The study has used data recorded by an on-board noise monitoring system during one year of traffic at the Stockholm metro.

The screening analysis showed that the occurrence of curve squeal increased with decreasing curve radius. In addition, the results showed the occurrence of curve squeal to be:

- reduced during precipitation,
- unrelated to the location of the curve inside or outside of tunnels, apart from the relation mentioned above,
- unrelated to the application of high rail lubrication,
- not significantly influenced by vehicle speed for the measured variation range (around 10km/h),
- increased for moderate temperatures between 4^oC and 16 ^{o}C,
- increased with increased relative humidity for the 122 m radius curve. A similar relation for the investigated 318 m radius curve was not found.

The observations regarding the influence of humidity and precipitation on the occurrence of curve squeal indicate the importance of the wheel–rail friction coefficient for its generation.

The model selected for the logistic regression analysis is a compromise between that providing the best fit and the model that imitates a behaviour closest to what is expected and that is consistent with the measurement data. For the current study, the model that showed the best physical behaviour for curve squeal with respect to the predictor variables was considered to be the most appropriate choice. In particular, the significantly better behaviour of the chosen model for predictor variable combinations corresponding to few measured observations was considered an advantage over the slightly better accuracy of the model that had the best overall fit. Results predicted with the logistic regression model should be used with caution outside the areas with plenty of observations.

5.1 Future work

The current work has shown that the influence of the predictor variables on the generation of curve squeal varied between the two investigated curves of different radii. Based on this observation, it is suggested to expand the methodology proposed in the current work for the logistic regression analysis to account for more curves capturing a larger range of curve radii. This could provide valuable knowledge and a comprehensive basis for future strategic work on methods to mitigate the generation of curve squeal on the Stockholm metro.

The project has a potential to deepen the knowledge about curve squeal and flanging noise generation. The latter could be captured from the data collected by the on-board noise monitoring system by applying an appropriate criterion. Potentially a criterion to identify and differentiate brake squeal as a separate noise source could be developed. In addition, the generation of impact noise and how it is influenced by operative conditions could be included in the investigation.

References

[1] Hanson, D., Jiang, J., Dowdell, B., Dwight, R.:*Curve Squeal: Causes, Treatments and Results*. In INTER-NOISE, Melbourne, Australia, 2014.

[2] Nilsson, R., Bergseth, E., Lyu, Y., Björklund, S., Olofsson, U., Lindgren, A., Höjer, M.: *Development of a noise related track maintenance tool. Wheel flange/rail gauge corner wear and lubrication.*, Proceedings of 22nd International Congress on Sound and Vibration, Florence, Italy, 2015.

[3] Thompson, D. J., Squicciarini, G., Ding, B., Baeza, L.: *A state-of-art review of curve squeal noise: phenomena, mechanisms, modelling and mitigation.* Notes on Numerical Fluid Mechanics and Multidisciplinary Design. Cham. Springer, pp. 3-41.

[4] Remington, P. J.: *Wheel/rail squeal and impact noise: What do we know? What don't we know? Where do we go from here?*, Journal of Sound and Vibration 116(2), 339-353 (1987)

[5] Thompson, D. J.: Curve Squeal Noise, In Thompson, D. J.: *Railway Noise and Vibrations: Mechanisms, Modelling and Mitigation*, chapter 9, pages 315 – 342. Elsevier: Oxford, (2009).

[6] Eadie D, Santoro M. Kalousek, J.: *Railway noise and the effect of top of rail liquid friction modifiers: changes in sound and vibration spectral distributions.* Proceedings of 6th International Conference on Contact Mechanics and Wear of Rail/Wheel Systems, 2003

[7] Gelfand, S.,A.:*Hearing. An Introduction to Psychological and Phusiological Acoustics*, 5^{th} Edition , chapter 11, Informa Healthcare, UK, (2010)

[8] Nelson, J. T.: *Transport Cooperative Research Program, Report 23: Wheel/rail Noise Control Manual.* Transportation Research Board, pp. 54-65. National Academy Press, Washington D.C. (1997)

[9] Oertli, J.: *Combatting curve squeal, phase II, final report*, UIC (2005)

[10] Bullen, R., Jiang, J.: *Algorithms for detection of rail wheel squeal.* Proceedings of 20th International Congress on Acoustics 2010, ICA 2010 - Incorporating Proceedings of the 2010 Annual Conference of the Australian Acoustical Society. pp. 2212-2216 (2010)

[11] Wickens, A. H.: *Fundamentals of Rail Vehicle Dynamics, Guidance and Stability*, Sweets & Zeitlinger, Lisse, (2003).

[12] Rudd, M. J.: *Wheel/rail noise – Part II: Wheel squeal*, Journal of Sound and Vibration 46(3), 381 – 394, (1976).

[13] Torstensson, P.: *Rail Corrugation Growth on Curves. Section 5: Curving behavior of railway bogies.* Ph. D. Dissertation, Department of Applied Mechanics, Chalmers University of Technology, Göteborg, Sweden (2012).

[14] Andersson, E., Berg, M., Stichel, S.: *Rail Vehicle Dynamics.*, Stockholm, 2007

[15] Fourie, D. J., Gräbe, P. J., Heyns, P. S., Fröhling, R. D.: *Experimental characterisation of railway wheel squeal occurring in large – radius curves.* Proceedings of the Institution of Mechanical Engineers, Part F: Journal of Rail and Rapid Transit, 230(6) 1561 – 1574 (2016)

[16] Ding, B., Squicciarini, G., Thompson, D. J., Corradi, R.: *An assessment of mode-coupling and falling-friction mechanisms in railway curve squeal through a simplified approach.* Journal of Sound and Vibration, 423, 126-140 (2018)

[17] Verheijen, E., van Haaren, E..: *A measurement protocol for curve squeal noise*, AEA Technology Rail BV, Concordiastraat 67, 3551 EM Utrecht, Netherlands

[18] Anderson, D.:*Wheel squeal measurement, management and mitigation on the New South Wales Rail Network.* Proceedings of ACOUSTICS 2004, Australia

[19] Koch, J. R., Vincent, N., Chollet, H., Chiello, O.: *Curve squeal of urban rolling stock – Part 2: Parametric study on a ¼ scale test rig.* Journal of Sound and Vibration 293(3), 701-709 (2006)

[20] Vincent, N., Koch, J. R., Chollet, H., Guerder, J. Y.: *Curve squeal of urban rolling stock – Part 1: State of art and field measurements.* Journal of Sound and Vibration 293(3), 691 – 700 (2006)

[21] Jiang, J., Dwight, R., Anderson, D.:*Field verification of curving noise mechanisms. In Maeda, T., et al. (eds.) Noise and Vibration Mitigation*

for Rail Transportation Systems. NNFM, vol. 126, pp. 587-594. Springer, Heidelberg (2015)

[22] Anderson, D., Wheatley, N., Fogarty, B., Jiang, J., Howie, A., Potter, W.:*Mitigation of Curve Squeal Noise in Queensland, New South Wales and South Australia.* Proceedings of Conference of Railway Engineering. pp. 625 – 636, Perth, Australia (2008)

[23] De Beer, F. G., Janssens, M. H. A., Kooijman, P. P.: *Squeal noise of rail-bound vehicles influenced by lateral contact position.* Journal of Sound and Vibration 267(3), 497-507 (2003)

[24] Liu, X., Meehan, P. A.:*Investigation of squeal noise under positive friction characteristics condition provided by friction modifiers.* Journal of Sound and Vibration 371, 393-405 (2016)

[25] Corradi, R., Crosio, P., Manzoni, S., Squicciarini, G.: *Experimental investigation on squeal noise in tramway sharp curves.* Proceedings of the 8th International Conference on Structural Dynamics, EURODYN 2011, Leuven, Belgium.

[26] Liu, X., Meehan, P. A.: *Investigation of the effect of relative humidity on lateral force in rolling contact and curve squeal.* Wear 310(1), 12-19 (2014)

[27] Meehan, P.A., Bellette, P.A. Jones, C., Anderson, D.: *Probabilistic prediction of wheel squeal under eld humidity variation.* Proceedings of 20th International Congress on Acoustics, ICA 2010, Sydney, Australia, 2010.

[28] Craven, N. (coordinator): UIC Noise Technical Measures Catalogue, International Union of Railways, May 2013.

[29] Liu, B., Mei, T. X., Bruni, S.: *Design and optimisation of wheel–rail profiles for adhesion improvement*, Vehicle System Dynamics, 54:3, 429-444, *DOI* : 10.1080/00423114.2015.1137958 (2016)

[30] https://cordis.europa.eu/project/rcn/109752/factsheet/en, (access: 2019-11-13)

[31] Höjer, M., Almgren, M.: *Monitoring system for track roughness*, EuroNoise, Maastricht, 2015

[32] https://www.bombardier.com/en/transportation.html, (access: 2019-11-13)

[33] Peng, C.-Y.J., Lee, K.L.,Ingersoll, G.M.: *An Introduction to Logistic Regression Analysis and Reporting*, Indiana University - Bloomington, The

Journal of Educational Research 96(1):3-14, September 2002

[34] Ranstam, J., *Why the P-value culture is bad and confidence intervals a better alternative*, Osteoarthritis and Cartilage, 2012. 20 (8): 805–808.

[35] Altman, D.G., Bland, M.: *Statistics notes: absence of evidence is not evidence of absence*,BMJ, 311 (1995), p. 485

[36] https://www.smhi.se/

[37] https://www.r-project.org/

[38] Collett, D.:*Modelling Binary Data*, Chapman and Hall/CRC; 1st edition (October 1, 1991), p. 53-56.

[39] King, G.: Unifying Political Methodology : *The Likelihood Theory of Statistical Inference.* New York: Cambridge University Press, 1989. p. 84

[40] Ng, A.: Machine Learning, online course:
https://www.coursera.org/learn/machine-learning (access: 2019-04-29)

A

Appendix

A.1 Detailed time and weather conditions

Table A.1: Detailed information about time and weather conditions during 3 passages through the 122 m radius curve between Alvik and Stora mossen, presented in Figure 4.1 and Figure 4.2

Condition	Curve Squeal	Flanging noise with less severe squeal	Without squeal
Speed	35.5km/h	33.7km/h	29.3km/h
Humidity	83%	70%	93%
Temperature	7.4^oC	7.8^oC	8.3^oC
Precipitation	3.6mm	0mm	16.5mm
Date	2017-10-11, 22:29	2017-10-10, 17:11	2017-10-08, 21:57

Table A.2: Detailed information about time and weather conditions during 3 passages through 3 different curves, presented in Figure 4.6 and Figure 4.7

Condition	R=122 m, ALV-SMO	R = 150 m, SKB-GUP	R = 318 m, ALV-SMO
Speed	34.7km/h	28.5km/h	36.5km/h
Humidity	90%	83%	98%
Temperature	15.1^oC	-7.8^oC	-5.5^oC
Precipitation	0.2 mm	0 mm	0 mm
Date	2017-09-23, 13:15	2018-03-04, 21:28	2018-01-22, 18:44

A.2 Documentation of the studied part of green line

Category	Part	Section	Curve	Distance from reference station in m	Curve Radius in m	Lubrication at X m from reference station	Tunnel
1	SLUSEN - HÄSSELBY STRAND	336	1	8375	-115		
		337		8400	-115		
		338		8425	-115		
		339		8450	-115		
		340	2	8475	122		
		341		8500	122		
		342		8525	122		
		343		8550	122		
		344		8575	122		
		345		8600	122		
		346		8625	122		
		347		8650	122	8668	
		348		8675	122	8668	
	SLUSEN - SKÄRMARBRINK	1598	3	-2425	-150		
		1599		-2450	-150		
		1600		-2475	-150	-2599	
		1601		-2500	-150	-2599	
		1602		-2525	-150	-2599	
		1603		-2550	-150	-2599	
		1604		-2575	-150	-2599	
		1605		-2600	-150		
	GULMARSPLAN-HAGSÄTRA	2782	4	-2400	160		
		2783		-2425	160		
		2784		-2450	160	-2561	
		2785		-2475	160	-2561	
		2786		-2500	160	-2561	
		2787		-2525	160	-2561	
		2788		-2550	160	-2561	
		2802	5	-2900	190		

Figure A.1: Documentation of the northbound part of the green line at SL. Category 1.

Category	Part	Section	Curve	Distance from reference station in m	Curve Radius in m	Lubrication at X m from reference station	Tunnel
2	SLUSEN - HÄSSELBY STRAND	51	1	1250	213		1
		52		1275	213		1
		53		1300	213		1
		54		1325	213		1
		55		1350	213		1
		56		1375	213		1
		57		1400	213		1
		58		1425	213		1
		59		1450	213		1
		68	2	1675	-213	1666	1
		69		1700	-213	1666	1
		70		1725	-213	1666	1
		71		1750	-213	1666	1
		72		1775	-213	1666	1
		73		1800	-213	1666	1
		74		1825	-213		1
		75		1850	-213		1
		76		1875	-213		1
		77		1900	-213		1
		78		1925	-213		1
		79		1950	-213		1
		125	3	3100	-221		1
		126		3125	-221		1
		127		3150	-221		1
		153	4	3800	-200		1
		154		3825	-200		1
		155		3850	-200		1
		156		3875	-200		1
		157		3900	-200		1
		158		3925	-200		1
		159		3950	-200		1
		160		3975	-200		1
		161		4000	-200		1
		162		4025	-200		1
		163		4050	-200		1

Figure A.2: Documentation of the northbound part of the green line at SL. Category 2

2	SLUSEN - HÄSSELBY STRAND	198	5	4925	265	4938	1
		199		4950	265	4938	1
		200		4975	265	4938	1
		201		5000	265	4938	1
		333	6	8300	-244	8272	
		334		8325	-244	8272	
		335		8350	-244	8272	
	SLUSEN - SKÄRMARBRINK	1515	7	-350	270		1
		1516		-375	270		1
		1517		-400	270		1
	SKÄRMARBRINK-SKARPNÄCK	2353	8	-3175	261		
		2354		-3200	261		
		2355		-3225	261		
		2356		-3250	261		
		2357		-3275	261		
		2358		-3300	261		
		2359		-3325	261		
		2360		-3350	261		
	SKÄRMARBRINK-FARSTA STRAND	1627	9	-3150	222		
		1628		-3175	222		
		1629		-3200	222		
		1630		-3225	222	-3365	
		1631		-3250	222	-3365	
		1632		-3275	222	-3365	
		1633		-3300	222	-3365	
	GULLMARSPLAN-HAGSÄTRA	2790	10	-2600	-203		
		2797	11	-2775	200		
		2798		-2800	200		
		2799		-2825	200		
		2800		-2850	200		
		2801		-2875	200		
		2803	12	-2925	208	-3120	
		2804		-2950	208	-3120	
		2836	13	-3750	-266	-3890	
		2837		-3775	-266	-3890	
		2847	14	-4025	230		
		2848		-4050	230		
		2849		-4075	230		
		2850		-4100	230		
		2851		-4125	230		
		2852		-4150	230		
		2853		-4175	230		
		2854		-4200	230	-4332	
		2855		-4225	230	-4332	
		2856		-4250	230	-4332	
		2857		-4275	230	-4332	

Figure A.3: Documentation of the northbound part of the green line at SL. Category 2

Category	Part	Section	Curve	Distance from reference station in m	Curve Radius in m	Lubrication at X m from reference station	Tunnel
3	SLUSEN - HÄSSELBY STRAND	1	1	0	390		1
		2		25	390		1
		3		50	390		1
		4		75	390		1
		18	2	425	394		1
		19		450	394		1
		20		475	394		1
		21		500	394		1
		115	3	2850	-350	2721	1
		116		2875	-350		1
		117		2900	-350		1
		118		2925	-350		1
		119		2950	-350		1
		120		2975	-350		1
		121	4	3000	-358		1
		122		3025	-358		1
		123		3050	-358		1
		124		3075	-358		1
		193	5	4800	-370		1
		194		4825	-370		1
		195		4850	-370		1
		196		4875	-370		1
		202	6	5025	308	4938	1
		203		5050	308	4938	1
		204		5075	308		1
		205	7	5100	398		1
		206		5125	398		1
		207		5150	398		1
		208		5175	398		1
		209		5200	398		1
		210		5225	398		1
		211		5250	398		1
		212		5275	398		1
		213		5300	398		1
		214		5325	398		1

Figure A.4: Documentation of the northbound part of the green line at SL. Category 3

3	SLUSEN - HÄSSELBY STRAND	282	8	7025	-375		
		283		7050	-375		
		284		7075	-375		
		285		7100	-375		
		295	9	7350	-323		
		296		7375	-323		
		297		7400	-323		
		298		7425	-323		
		299		7450	-323		
		309	10	7700	300	7615	
		310		7725	300		
		311		7750	300		
		312		7775	300		
		349	11	8700	-318		
		350		8725	-318	8738	
		351		8750	-318	8738	
		352		8775	-318		
		353		8800	-318		
		354		8825	-318		
		355		8850	-318		
		420	12	10475	333		
		421		10500	333		
		422		10525	333		
		423		10550	333		
		424		10575	333		
		425		10600	333		
		492	13	12275	398		
		493		12300	398		
		494		12325	398		
		495		12350	398		
		496	13	12375	398		
		497		12400	398		
		498		12425	398		
		499		12450	398		
		500		12475	398		
		501		12500	398		
		502		12525	398		
		563	14	14050	383		
		564		14075	383		
		565		14100	383		
		566		14125	383		
		567		14150	383		
		568		14175	383		
		569		14200	383		
		570		14225	383		
		571		14250	383		
		572		14275	383		
		573		14300	383		
		574		14325	383		
		575		14350	383		

Figure A.5: Documentation of the northbound part of the green line at SL. Category 3

3	SLUSEN - SKÄRMARBRINK	1502	15	-25	394		1
		1509	16	-200	-323	-293	1
		1510		-225	-323	-293	1
		1511		-250	-323	-293	1
		1524	17	-575	-398	-680	1
		1525		-600	-398	-680	1
		1526		-625	-398	-680	1
		1587	18	-2150	300		
		1588		-2175	300		
		1589		-2200	300		
		1590	19	-2225	-365		
		1591		-2250	-365		
		1592		-2275	-365		
		1613	20	-2800	340		
		1614		-2825	340		
		1616	21	-2875	300		
		1617	22	-2900	312		
		1618		-2925	312		
		1619		-2950	312		
	SKÄRMARBRINK-SKARPNÄCK	2398	24	-4300	364		
		2399		-4325	364		
		2400		-4350	364		
		2401		-4375	364		
		2402	25	-4400	307		
		2403		-4425	307		
		2404		-4450	307		
		2405		-4475	307		
		2406		-4500	307		
		2407		-4525	307		
		2408		-4550	307		
		2409		-4575	307		
		2410		-4600	307		
		2411		-4625	307		
	SKÄRMARBRINK-FARSTA STRAND	1626	26	-3125	300		
		1711	27	-5250	300		
		1712		-5275	300		
		1713		-5300	300		
		1714		-5325	300		
		1715		-5350	300		
		1716		-5375	300		
		1717		-5400	300		
		1718		-5425	300		
		1804	28	-7575	-399		
		1805		-7600	-399		
		1806		-7625	-399		
		1816	29	-7875	-387		
		1817		-7900	-387		
		1818		-7925	-387		
		1899	30	-9950	-354		1
		1900		-9975	-354		1

Figure A.6: Documentation of the northbound part of the green line at SL. Category 3

3	SKÄRMARBRINK-FARSTA STRAND	1901	30	-10000	-354		1
		1902		-10025	-354		1
		1903		-10050	-354		1
		1904		-10075	-354		1
		1905		-10100	-354		1
		1906		-10125	-354		1
		1911	31	-10250	-343		1
		1912		-10275	-343		1
	GULLMARSPLAN-HAGSÄTRA	2776	32	-2250	-378		
		2777		-2275	-378		
		2791	33	-2625	-389		
		2792		-2650	-389		
		2793	34	-2675	-399		
		2794		-2700	-399		
		2795		-2725	-399		
		2812	35	-3150	370		
		2813		-3175	370		
		2814		-3200	370		
		2815	36	-3225	-391		
		2816		-3250	-391		
		2817		-3275	-391		
		2818		-3300	-391		
		2819		-3325	-391		
		2820		-3350	-391		
		2821		-3375	-391		
		2822		-3400	-391		
		2823		-3425	-391		
		2827	37	-3525	-311		
		2828		-3550	-311		
		2829		-3575	-311		
		2830		-3600	-311		
		2831		-3625	-311		
		2832		-3650	-311		
		2833		-3675	-311		
		2834		-3700	-311		
		2835	38	-3725	-398		
		2875	39	-4725	-366		
		2876		-4750	-366		
		2877		-4775	-366		
		2878		-4800	-366		
		2882	40	-4900	398		
		2883		-4925	398		
		2884	41	-4950	300		
		2885		-4975	300		
		2886		-5000	300		
		2887	42	-5025	312		
		2888		-5050	312		
		2889		-5075	312		
		2890	43	-5100	322		
		2891		-5125	322		

Figure A.7: Documentation of the northbound part of the green line at SL. Category 3

3	GULLMARSPLAN-HAGSÄTRA	2925	44	-5975	-302		
		2926		-6000	-302		
		2927		-6025	-302		
		2928		-6050	-302		
		2929		-6075	-302		
		2930		-6100	-302		
		2931		-6125	-302		
		2932		-6150	-302		
		2933		-6175	-302		
		2934		-6200	-302		
		2935		-6225	-302		
		2936		-6250	-302		
		2937		-6275	-302		
		2938		-6300	-302		

Figure A.8: Documentation of the northbound part of the green line at SL. Category 3

Category	Part	Section	Cvurve	Distance from reference station in m	Curve Radius in m	Lubrication at X m from reference station	Tunnel
4	SLUSEN - HÄSSELBY STRAND	16	1	375	421		1
		17		400	421		1
		250	2	6225	433		
		251		6250	433		
		252		6275	433		
		253		6300	433		
		254		6325	433		
		255		6350	433		
		403	3	10050	-419		
		404		10075	-419		
		405	4	10100	-404		
		406		10125	-404		
		407		10150	-404		
		408		10175	-404		
		409		10200	-404		
		456	5	11375	-465		
		457		11400	-465		
		458		11425	-465		
		459		11450	-465		
		475	6	11850	-453		
		476		11875	-453		
		525	7	13100	-449		
		526		13125	-449		
		527		13150	-449		
		528		13175	-449		
		529		13200	-449		
		530		13225	-449		
	SLUSEN - SKÄRMARBRINK	1503	8	-50	400		1
		1504		-75	400		1
	SKÄRMARBRINK- SKARPNÄCK	2451	9	-5625	-450		
		2452		-5650	-450		
		2453		-5675	-450		
	SKÄRMARBRINK- FARSTA STRAND	1662	10	-4025	-476		
		1663		-4050	-476		
		1692	11	-4775	424		
		1693		-4800	424		
		1694		-4825	424		
		1695		-4850	424		
		1696		-4875	424		
		1697		-4900	424		
		1698		-4925	424		
		1807	12	-7650	-406		

Figure A.9: Documentation of the northbound part of the green line at SL. Category 4

4	SKÄRMARBRINK-FARSTA STRAND	1808	13	-7675	-401		
		1809		-7700	-401		
		1810		-7725	-401		
		1811		-7750	-401	-7861	
		1812		-7775	-401	-7861	
		1813		-7800	-401	-7861	
		1827	14	-8150	464		
		1828		-8175	464		
		1829		-8200	464		
		1830		-8225	464		
		1831		-8250	464		
		1832		-8275	464		
		1890	15	-9725	497		1
		1891		-9750	497		1
		1892		-9775	497		1
		1893		-9800	497		1
		1894		-9825	497		1
		1895		-9850	497		1
		1896		-9875	497		1
	GULLMARSPLAN-HAGSÄTRA	2838	16	-3800	-482	-3890	
		2839		-3825	-482	-3890	
		2869	17	-4575	-425		
		2870		-4600	-425		
		2871		-4625	-425		
		2872		-4650	-425		
		2873		-4675	-425		
		2874		-4700	-425		
		3031	18	-8625	423		
		3032		-8650	423		
		3033		-8675	423		
		3034		-8700	423		
		3035		-8725	423		
		3036		-8750	423		
		3037		-8775	423		
		3038		-8800	423		
		3039		-8825	423		
		3040		-8850	423		
		3041		-8875	423		
		3042		-8900	423		
		3043	19	-8925	447		
		3044	20	-8950	417		
		3045		-8975	417		
		3046		-9000	417		
		3047		-9025	417		
		3048		-9050	417		
		3049		-9075	417		
		3050		-9100	417		
		3051		-9125	417		

Figure A.10: Documentation of the northbound part of the green line at SL. Category 4

Category	Part	Section	Curve	Distance from reference station in m	Curve Radius in m	Lubrication at X m from reference station	Tunnel
5	SLUSEN - HÄSSELBY STRAND	8	1	175	650		
		9		200	650		
		23	2	550	583		1
		24		575	583		1
		25		600	583		1
		26		625	583		1
		27		650	583		1
		28	3	675	606		1
		29		700	606		1
		30		725	606		1
		31		750	606		1
		32		775	606		1
		33		800	606		1
		43	4	1050	583		1
		44		1075	583	1075	1
		45		1100	583	1075	1
		46		1125	583	1075	1
		47		1150	583	1075	1
		48		1175	583		1
		49		1200	583		1
		50		1225	583		1
		60	5	1475	567		1
		61		1500	567		1
		62		1525	567		1
		63		1550	567		1
		64		1575	567		1
		65		1600	567		1
		66		1625	567	1629	1
		92	6	2275	-670		1
		93		2300	-670		1
		94		2325	-670		1
		111	7	2750	-596	2721	1
		112		2775	-596	2721	1
		113		2800	-596	2721	1
		114		2825	-596	2721	1
		131	8	3250	-665		1
		132		3275	-665		1
		133		3300	-665		1

Figure A.11: Documentation of the northbound part of the green line at SL. Category 5

5	SLUSEN - HÄSSELBY STRAND	134	9	3325	547		1
		135		3350	547		1
		217	10	5400	599		1
		218		5425	599		1
		219		5450	599		1
		416	11	10375	625		
		417		10400	625		
		418		10425	625		
		419		10450	625		
		426	12	10650	664		
		434	13	10825	-539		
		435		10850	-539		
		436		10875	-539		
		437		10900	-539		
		454	14	11325	-599		
		455		11350	-599		
		506	15	12625	663		
		507		12650	663		
		508		12675	663		
		509		12700	663		
		553	16	13800	502		1
		554		13825	502		1
		555		13850	502		1
		556		13875	502		1
		557		13900	502		1
		558		13925	502		1
		559		13950	502		1
		560		13975	502		1
		576	17	14375	582		
		577		14400	582		
		578		14425	582		
		616	18	15375	-650		
		617		15400	-650		
		618		15425	-650		
		619		15450	-650		
		620		15475	-650		
		627		15650	-650		
		628		15675	-650		
		660	19	16475	-515		
		661		16500	-515		
		662		16525	-515		
		663		16550	-515		
		664		16575	-515		
		665		16600	-515		
		666		16625	-515		
		667		16650	-515		
		668		16675	-515		
		669		16700	-515		

Figure A.12: Documentation of the northbound part of the green line at SL. Category 5

5	SLUSEN - HÄSSELBY STRAND	733	20	18300	-627		
		734		18325	-627		
		735		18350	-627		
		736		18375	-627		
		737		18400	-627		
		738		18425	-627		
		743	21	18550	-650		
		744		18575	-650		
	SLUSEN - SKÄRMARBRINK	1514	22	-325	527		1
		1544	23	-1075	600		1
		1547	24	-1150	-667		1
		1554	25	-1325	619		1
		1560	26	-1475	-669		1
		1561		-1500	-669		1
		1606	27	-2625	504		
		1607		-2650	504		
		1608	28	-2675	-500		
		1609		-2700	-500		
		1620	29	-2975	521		
		1621		-3000	521		
	SKÄRMARBRINK- SKARPNÄCK	2422	30	-4900	568		
		2423	31	-4925	654		
		2424		-4950	654		
		2425		-4975	654		
		2439	32	-5325	-511		
		2440		-5350	-511		
		2441		-5375	-511		
		2442		-5400	-511		
		2443		-5425	-511		
		2448	33	-5550	-540		
		2449		-5575	-540		
		2450		-5600	-540		
		2471	34	-6125	570		
		2472		-6150	570		
		2473		-6175	570		
		2474		-6200	570		
		2475		-6225	570		
		2476		-6250	570		
		2477		-6275	570		
		2478		-6300	570		
		2479		-6325	570		
		2480		-6350	570		
		2481		-6375	570		
		2482		-6400	570		1
		2483		-6425	570		1
		2491	35	-6625	600		1
		2492		-6650	600		1
		2493		-6675	600		1

Figure A.13: Documentation of the northbound part of the green line at SL. Category 5

5	SKÄRMARBRINK-SKARPNÄCK	2494	35	-6700	600		1
		2495		-6725	600		1
		2496		-6750	600		1
		2497		-6775	600		1
		2498		-6800	600		1
		2499		-6825	600		1
		2500		-6850	600		1
		2501		-6875	600		1
		2502		-6900	600		1
		2513	36	-7175	570		1
		2514		-7200	570		1
		2515		-7225	570		1
		2516		-7250	570		1
		2517		-7275	570		1
		2518		-7300	570		1
		2519		-7325	570		1
		2520		-7350	570		1
		2521		-7375	570		1
		2522		-7400	570		1
		2523		-7425	570		1
		2524		-7450	570		1
		2525		-7475	570		1
		2526		-7500	570		1
	SKÄRMARBRINK-FARSTA STRAND	1649	37	-3700	-624		
		1650		-3725	-624		
		1651		-3750	-624		
		1748	38	-6175	-514		
		1749		-6200	-514		
		1750		-6225	-514		
		1751		-6250	-514		
		1752		-6275	-514		
		1753		-6300	-514		
		1754		-6325	-514		
		1824	39	-8075	599		
		1825		-8100	599		
		1826	40	-8125	609		

Figure A.14: Documentation of the northbound part of the green line at SL. Category 5

5	GULLMARSPLAN-HAGSÄTRA	2805	41	-2975	579	-3120	
		2806		-3000	579	-3120	
		2807		-3025	579	-3120	
		2808	42	-3050	695	-3120	
		2809		-3075	695	-3120	
		2824	43	-3450	600		
		2825		-3475	600		
		2826		-3500	600		
		2903	45	-5425	650		
		2904		-5450	650		
		2905		-5475	650		
		2906		-5500	650		
		2957	46	-6775	629		
		2958		-6800	629		
		2959		-6825	629		
		2960		-6850	629		
		2961		-6875	629		
		2962		-6900	629		
		2963		-6925	629		
		2964		-6950	629		
		2965		-6975	629		
		2966		-7000	629		
		2991	47	-7625	505		
		2992		-7650	505		
		2993		-7675	505		
		2994		-7700	505		
		2995		-7725	505		
		2996		-7750	505		
		2997		-7775	505		
		2998		-7800	505		
		2999		-7825	505		
		3000		-7850	505		
		3001		-7875	505		
		3002		-7900	505		
		3003		-7925	505		
		3004		-7950	505		
		3052	48	-9150	639		
		3053		-9175	639		
		3054		-9200	639		
		3055		-9225	639		
		3056		-9250	639		
		3057		-9275	639		
		3058		-9300	639		
		3059		-9325	639		
		3060		-9350	639		
		3061		-9375	639		
		3062		-9400	639	-9587	
		3063		-9425	639	-9587	
		3064		-9450	639	-9587	
		3065		-9475	639	-9587	
		3066		-9500	639	-9587	
		3067		-9525	639	-9587	

Figure A.15: Documentation of the northbound part of the green line at SL. Category 5

Category	Part	Section	Curve	Distance from reference station in m	Curve Radius in m	Lubrication at X m from reference station	Tunnel
6	SLUSEN - HÄSSELBY STRAND	38	1	925	795		1
		39		950	795		1
		40		975	795		1
		146	2	3625	808		1
		147		3650	808		1
		151	3	3750	835		1
		152		3775	835		1
		215	4	5350	706		1
		216		5375	706		1
		237	5	5900	-877		
		238		5925	-877		
		239		5950	-877		
		246	6	6125	870		
		247		6150	870		
		300	7	7475	-900		
		301		7500	-900		
		306	8	7625	750	7615	
		307		7650	750	7615	
		308		7675	750	7615	
		395	9	9850	870		
		410	10	10225	-836		
		411		10250	-836		
		412		10275	-836		
		452	11	11275	-862		
		453		11300	-862		
		513	12	12800	-786		
		514		12825	-786		
		537	13	13400	-900		1
		538		13425	-900		1
		587	14	14650	-787		
		588		14675	-787		
		589		14700	-787		
		590		14725	-787		
		602	15	15025	700		
		603		15050	700		
		604		15075	700		
		605		15100	700		
		606		15125	700		
		607		15150	700		
		608		15175	700		
		609		15200	700		
		610		15225	700		
		611		15250	700		
		612		15275	700		
		658	16	16425	-777		
		659		16450	-777		

Figure A.16: Documentation of the northbound part of the green line at SL. Category 6

6	SLUSEN - HÄSSELBY STRAND	716	17	17875	821		
		717		17900	821		
		718		17925	821		
		719		17950	821		
		720		17975	821		
	SLUSEN - SKÄRMARBRINK	1556	18	-1375	-708		1
		1578	19	-1925	800		
		1579		-1950	800		
	SKÄRMARBRINK-SKARPNÄCK	2427	20	-5025	782	-5107	
		2428		-5050	782	-5107	
		2444	21	-5450	-717		
		2445		-5475	-717		
		2446		-5500	-717		
	SKÄRMARBRINK-FARSTA STRAND	1770	22	-6725	-800		
		1771		-6750	-800		
		1772		-6775	-800		
		1861	23	-9000	-799		
		1862		-9025	-799		
		1863		-9050	-799		
		1864		-9075	-799		
		1865		-9100	-799		
		1866		-9125	-799		
		1867		-9150	-799		
		1868		-9175	-799		
		1869		-9200	-799		
		1887	24	-9650	865		1
		1888		-9675	865		1
		1889		-9700	865		1

Figure A.17: Documentation of the northbound part of the green line at SL. Category 6

6	GULLMARSPLAN-HAGSÄTRA	2892	25	-5150	873		
		2893		-5175	873		
		2894		-5200	873		
		2895		-5225	873		
		2912	26	-5650	840		
		2913		-5675	840		
		2914		-5700	840		
		2915		-5725	840		
		2916		-5750	840		
		2917		-5775	840		
		2918		-5800	840		
		2919		-5825	840		
		2920		-5850	840		
		2974	27	-7200	-756		
		2975		-7225	-756		
		2976		-7250	-756		
		2977	28	-7275	-870		
		2978		-7300	-870		
		2979		-7325	-870		
		3011	29	-8125	-795		
		3012		-8150	-795		
		3013		-8175	-795		
		3014		-8200	-795		
		3015		-8225	-795		
		3016		-8250	-795	-8345	
		3017		-8275	-795	-8345	
		3018		-8300	-795	-8345	
		3022	30	-8400	782		
		3023		-8425	782		
		3024		-8450	782		
		3075	31	-9725	-771		
		3076		-9750	-771		
		3077		-9775	-771		
		3078		-9800	-771		
		3079	32	-9825	-825		
		3080		-9850	-825		
		3081		-9875	-825		

Figure A.18: Documentation of the northbound part of the green line at SL. Category 6

A.3 Detailed screening analysis results

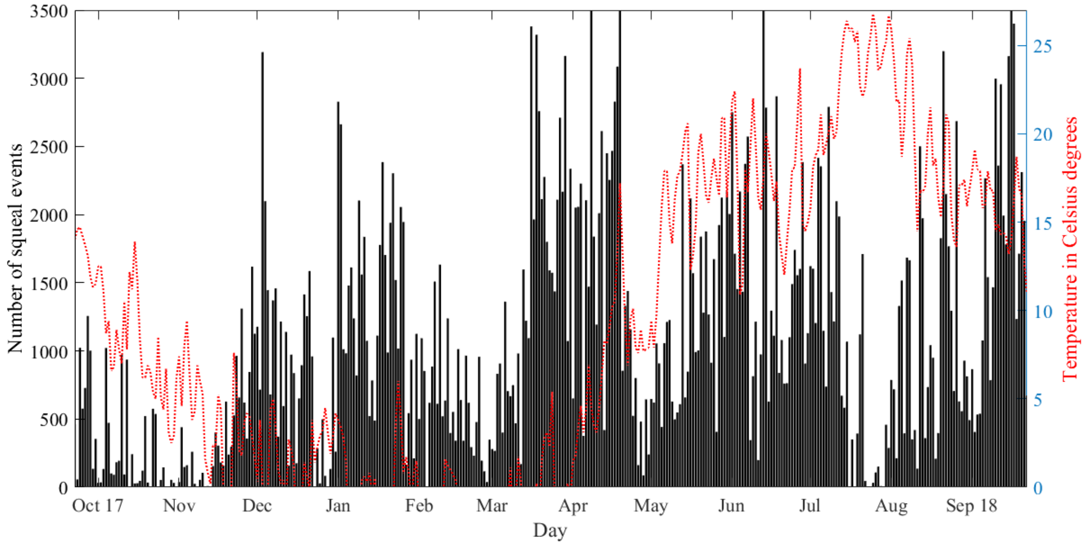

Figure A.19: Comparison between number of squeal events per day on the green metro line measured during period 2017-09-23 - 2018-09-23 and mean day temperature

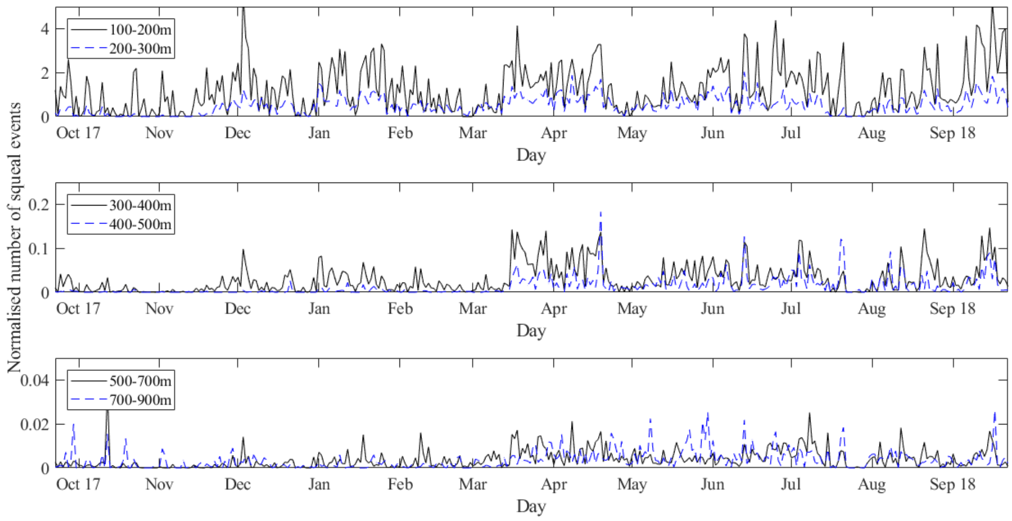

Figure A.20: Normalised number of squeal events per day on the green metro line measured during period 2017-09-23 - 2018-09-23 and divided into curve radius categories

A.4 Summary of data collected on the 318 m radius curve.

Data used in logistic regression for 318 m radius curve is summarised in Table A.3, A.4 and Table A.5, A.6 as well as in Figures A.21- A.22.

Table A.3: Summary of the classification data. Train data set collected on the northbound track at the 318 m radius curve located between stations Alvik and Stora mossen during the period 2017-08-25 - 2018-11-30

Curve Squeal	
Positive	406
Negative	386
Train data set size	792

Table A.4: Summary of the classification data. Test data set collected on the northbound track at the 318 m radius curve located between stations Alvik and Stora mossen during the period 2017-08-25 - 2018-11-30

Curve Squeal	
Positive	189
Negative	152
Test data set size	341

Table A.5: Summary of predictors. Train data set collected on the northbound track at the 318 m radius curve located between stations Alvik and Stora mossen during the period 2017-08-25 - 2018-11-30

Parameter	**Humidity**	**Temperature**
Unit	%	Celsius degrees
Min	23	-13.5
Max	100	31.1
Median	75	9.2
Mean	71.58	9.04
Standard deviation	19.71	9.59

Table A.6: Summary of predictors. Test data set collected on the northbound track at the 318 m radius curve located between stations Alvik and Stora mossen during the period 2017-08-25 - 2018-11-30

Parameter	**Humidity**	**Temperature**
Unit	%	Celsius degrees
Min	21	-10.4
Max	100	29.4
Median	75	9.6
Mean	70.91	9.88
Standard deviation	19.98	9.33

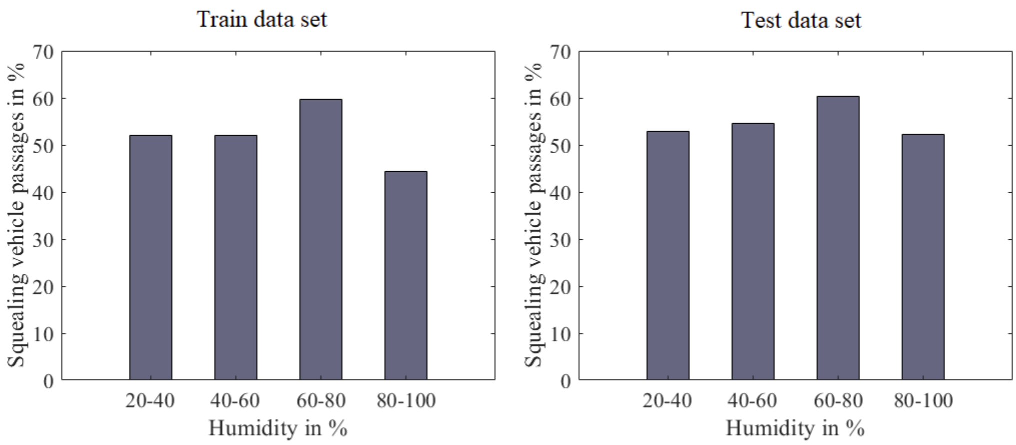

Figure A.21: Percentage squealing passages as a function of relative humidity. Train and test data sets collected on the northbound track at the 318 m radius curve located between stations Alvik and Stora mossen during the period 2017-08-25 - 2018-11-30

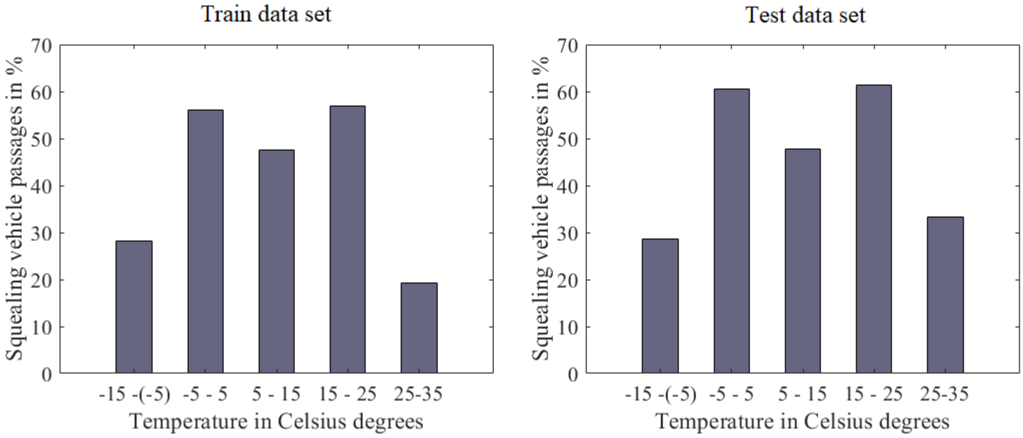

Figure A.22: Percentage squealing passages as a function of temperature. Train and test data sets collected on the northbound track at the 318 m radius curve located between stations Alvik and Stora mossen during the period 2017-08-25 - 2018-11-30

A.5 Logistic regression coefficients and odds ratios

Table A.7: Model coefficients of the logistic regression analysis of the 122 m radius curve located between stations Alvik and Stora mossen. The analysis performed on the train data set measured during the period 2017-08-25 - 2018-11-30 (model.a)

Coefficient	Parameter	Coefficient (θ_i)	Odds ratio ($exp(\theta_i)$)
θ_0	$X_0 = 1$	0.9638	2.6216
θ_1	X_2	-0.2263	0.7975
θ_2	X_3	0.5661	1.7614
θ_3	X_2^2	0.0050	1.0050
θ_4	X_3^2	-0.0286	0.9719
θ_5	X_2^3	-0.0000	1.0000
θ_6	X_3^3	0.0002	1.0002
θ_7	$X_2 \cdot X_3$	-0.0064	0.9937
θ_8	$X_2 \cdot X_3^2$	0.0003	1.0003

Table A.8: Model coefficients of the logistic regression analysis of the 122 m radius curve located between stations Alvik and Stora mossen. The analysis performed on the train data set measured during the period 2017-08-25 - 2018-11-30 (model.b)

Coefficient	Parameter	Coefficient (θ_i)	Odds ratio ($exp(\theta_i)$)
θ_0	$X_0 = 1$	-5.1354	0.0059
θ_1	X_2	0.1221	1.1298
θ_2	X_3	0.1503	1.1622
θ_3	X_2^2	-0.0007	0.9993
θ_4	X_3^2	-0.0004	0.9960
θ_5	$X_2 \cdot X_3$	-0.0012	0.9989

Table A.9: Model coefficients of the logistic regression analysis of the 318 m radius curve located between stations Alvik and Stora mossen. The analysis performed on the train data set measured during the period 2017-08-25 - 2018-11-30 (model.a)

Coefficient	Parameter	Coefficient (θ_i)	Odds ratio ($exp(\theta_i)$)
θ_0	$X_0 = 1$	3.863	47.6012
θ_1	X_2	-0.2781	0.7573
θ_2	X_3	0.5756	1.7783
θ_3	X_2^2	0.0055	1.0055
θ_4	X_3^2	-0.0277	0.9727
θ_5	X_2^3	-0.0000	1.0000
θ_6	X_3^3	0.0002	1.0002
θ_7	$X_2 \cdot X_3$	-0.0067	0.9934
θ_8	$X_2 \cdot X_3^2$	0.0003	1.0003

Table A.10: Model coefficients of the logistic regression analysis of the 318 m radius curve located between stations Alvik and Stora mossen. The analysis performed on the train data set measured during the period 2017-08-25 - 2018-11-30 (model.b)

Coefficient	Parameter	Coefficient (θ_i)	Odds ratio ($exp(\theta_i)$)
θ_0	$X_0 = 1$	-2.7732	0.0625
θ_1	X_2	0.1030	1.1085
θ_2	X_3	0.1777	1.1945
θ_3	X_2^2	-0.0008	0.9992
θ_4	X_3^2	-0.0006	0.9948
θ_5	$X_2 \cdot X_3$	-0.0010	0.9985

A.6 Logistic regression analysis results for 318 m radius curve

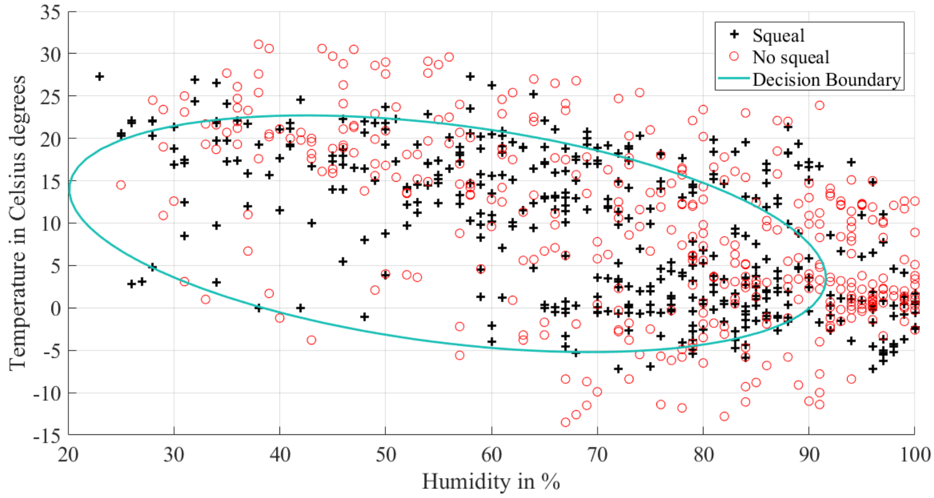

Figure A.23: Decision boundary plot obtained with the logistic regression model developed for the train data set collected on the northbound track at the 318 m radius curve located between stations Alvik and Stora mossen during the time period 2017-08-25 - 2018-11-30. Train data samples presented (model.b)

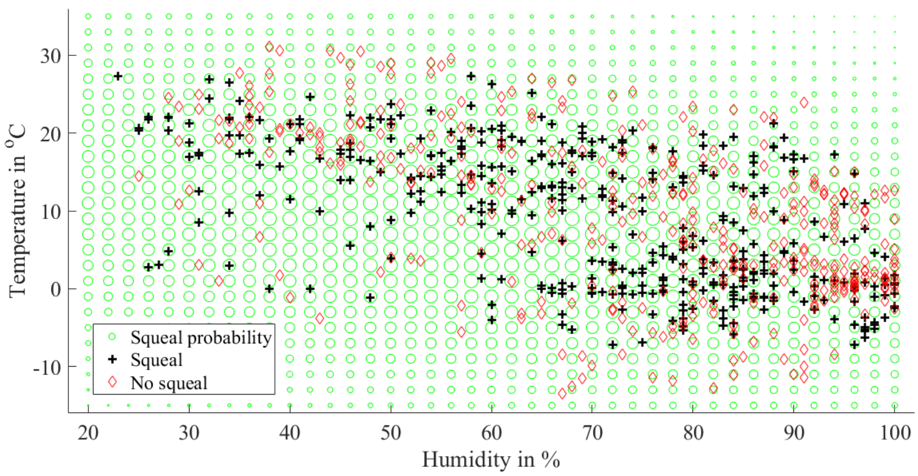

Figure A.24: Scatter plot with grid that indicates probability of squeal (green circles) obtained with the logistic regression model developed for the train data set collected on the northbound track at the 318 m radius curve located between stations Alvik and Stora mossen during the time period 2017-08-25 - 2018-11-30. Train data samples presented (model.b)

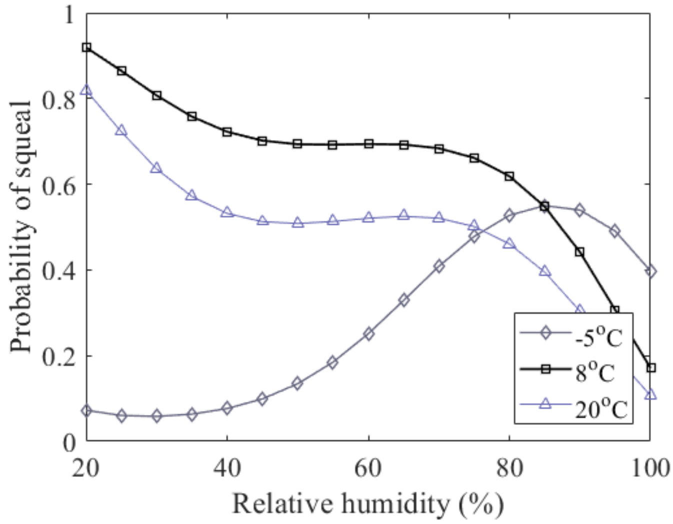

Figure A.25: The modelled influence of relative humidity for three different temperature values, obtained with the logistic regression model developed for the train data set collected on the northbound track at the 318 m radius curve located between stations Alvik and Stora mossen during the time period 2017-08-25 - 2018-11-30 (model.a)

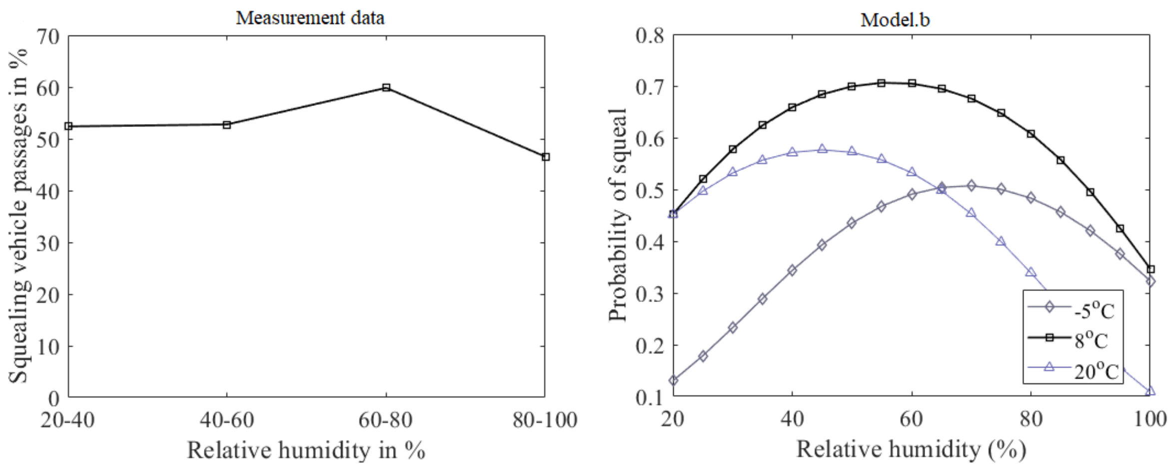

Figure A.26: The measured relation between the relative humidity and squeal occurrence based on the full data set and modelled relation between the relative humidity and squeal probability for three different temperature values obtained with the logistic regression model developed for the train data set collected on the northbound track at the 318 m radius curve located between stations Alvik and Stora mossen during the time period 2017-08-25 - 2018-11-30

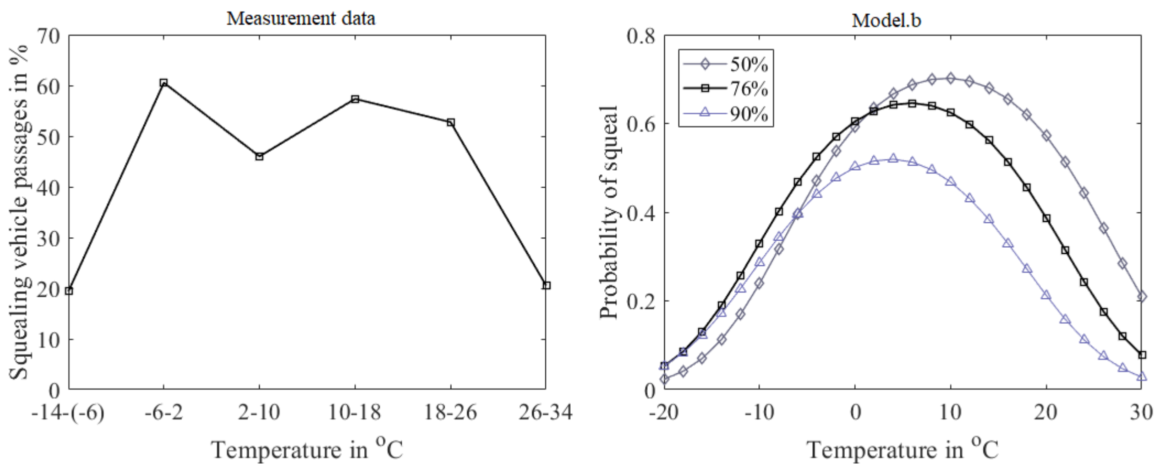

Figure A.27: The measured relation between the air temperature and squeal occurrence based on the full data set and modelled relation between the air temperature and squeal probability for three different humidity values obtained with the logistic regression model developed for the train data set collected on the northbound track at the 318 m radius curve located between stations Alvik and Stora mossen during the time period 2017-08-25 - 2018-11-30